

Water Resources Research



RESEARCH ARTICLE

10.1029/2021WR029844

Key Points:

- We explore the mobility of rhenium in three alpine catchments, in the context of its use as a proxy for rock organic carbon oxidation
- The relative abundance of dissolved Re increases with discharge, explained by a model where Re is mobilized from near surface zone
- The findings support rhenium as a proxy for oxidative weathering, and we find rock organic carbon oxidation increases with erosion rate

Supporting Information:

Supporting Information may be found in the online version of this article.

Correspondence to:

R. G. Hilton,
robert.hilton@earth.ox.ac.uk

Citation:

Hilton, R. G., Turowski, J. M., Winnick, M., Dellinger, M., Schleppe, P., Williams, K. H., et al. (2021). Concentration-discharge relationships of dissolved rhenium in alpine catchments reveal its use as a tracer of oxidative weathering. *Water Resources Research*, 57, e2021WR029844. <https://doi.org/10.1029/2021WR029844>

Received 18 FEB 2021
Accepted 26 OCT 2021

Author Contributions:










Conceptualization: Robert G. Hilton, Mathieu Dellinger

Data curation: Robert G. Hilton, Matthew Winnick, Mathieu Dellinger, Patrick Schleppe, Kenneth H. Williams, Corey R. Lawrence, Katharine Maher, Martin West, Amanda Hayton

Formal analysis: Robert G. Hilton, Matthew Winnick, Mathieu Dellinger, Patrick Schleppe, Corey R. Lawrence, Martin West, Amanda Hayton

Funding acquisition: Robert G. Hilton

Concentration-Discharge Relationships of Dissolved Rhenium in Alpine Catchments Reveal Its Use as a Tracer of Oxidative Weathering

Robert G. Hilton^{1,2} , Jens M. Turowski³ , Matthew Winnick⁴ , Mathieu Dellinger¹ , Patrick Schleppe⁵ , Kenneth H. Williams^{6,7} , Corey R. Lawrence⁸ , Katharine Maher⁹ , Martin West¹ , and Amanda Hayton¹

¹Department of Geography, Durham University, Science Laboratories, Durham, UK, ²Now at Department of Earth Sciences, University of Oxford, Oxford, UK, ³Helmholtz-Zentrum Potsdam, German Research Centre for Geosciences GFZ, Potsdam, Germany, ⁴Department of Geosciences, University of Massachusetts, Amherst, MA, USA, ⁵Swiss Federal Research Institute WSL, Birmensdorf, Switzerland, ⁶Lawrence Berkeley National Laboratory, Berkeley, CA, USA, ⁷Rocky Mountain Biological Lab, Gothic, CO, USA, ⁸Geosciences and Environmental Change Science Center, U.S. Geological Survey, Denver, CO, USA, ⁹Department of Earth System Science, Stanford University, Stanford, CA, USA

Abstract Oxidative weathering of sedimentary rocks plays an important role in the global carbon cycle. Rhenium (Re) has been proposed as a tracer of rock organic carbon (OC_{petro}) oxidation. However, the sources of Re and its mobilization by hydrological processes remain poorly constrained. Here, we examine dissolved Re as a function of water discharge, using samples collected from three alpine catchments that drain sedimentary rocks in Switzerland (Erlenbach and Vogelbach) and Colorado, USA (East River). The Swiss catchments reveal a higher dissolved Re flux in the catchment with higher erosion rates, but have similar [Re]/[Na⁺] and [Re]/[SO₄²⁻] ratios, which indicate a dominance of Re from OC_{petro}. Despite differences in rock type and hydro-climatic setting, the three catchments have a positive correlation between river water [Re]/[Na⁺] and [Re]/[SO₄²⁻] and water discharge. We propose that this reflects preferential routing of Re from a near-surface, oxidative weathering zone. The observations support the use of Re as a proxy to trace rock-organic carbon oxidation, and suggest it may be a hydrological tracer of vadose zone processes. We apply the Re proxy and estimate CO₂ release by OC_{petro} oxidation of 5.7^{+6.6}/_{-2.0} tC km⁻² yr⁻¹ for the Erlenbach. The overall weathering intensity was ~40%, meaning that the corresponding export of unweathered OC_{petro} in river sediments is large, and the findings call for more measurements of OC_{petro} oxidation in mountains and rivers as they cross floodplains.

Plain Language Summary When rocks undergo chemical weathering, breakdown of organic matter that has been stored in the rocks over time can release carbon dioxide to the atmosphere. It has remained a challenge to track and quantify this process, but the element rhenium provides a tool to do this. When organic matter in rocks undergoes oxidative weathering, rhenium is oxidized and enters river water. We can use measurements of dissolved rhenium fluxes as a proxy to estimate rock organic carbon oxidation. However, we still lack information on the sources of rhenium in river catchments and need a better understanding of the pathway that rhenium takes from rocks, through soils into streams and rivers. Here, we measured dissolved rhenium alongside other weathering products in three catchments that drain alpine landscapes made up of sedimentary rocks. The catchments behave in a remarkably similar way, where the relative amount of rhenium in river water increases with water flow. Based on our ideas of how water moves through the landscape, our results suggest that rhenium is moved from a near-surface zone in all three catchments, where oxygen and rock organic carbon react. By applying the proxy to the catchments, we confirm that oxidative weathering rates and their carbon dioxide release increase with physical erosion rates.

1. Introduction

When sedimentary rocks are exposed to oxygen in the atmosphere and hydrosphere, organic matter contained within the rocks can be oxidized (Petsch et al., 2000) and release carbon dioxide (CO₂) during “geo-respiration” (Keller & Bacon, 1998). Globally, the rates of CO₂ release to the atmosphere during oxidative weathering of rock-derived organic carbon (petrogenic OC and OC_{petro}) are thought to be ~40–100

© 2021. The Authors.

This is an open access article under the terms of the [Creative Commons Attribution](https://creativecommons.org/licenses/by/4.0/) License, which permits use, distribution and reproduction in any medium, provided the original work is properly cited.

Investigation: Robert G. Hilton, Jens M. Turowski, Matthew Winnick, Mathieu Dellinger, Katharine Maher

Methodology: Robert G. Hilton, Jens M. Turowski, Matthew Winnick, Mathieu Dellinger, Corey R. Lawrence, Martin West, Amanda Hayton

Project Administration: Robert G. Hilton

Resources: Robert G. Hilton, Jens M. Turowski, Patrick Schleppi, Kenneth H. Williams, Corey R. Lawrence, Katharine Maher

Validation: Robert G. Hilton

Visualization: Robert G. Hilton, Katharine Maher

Writing – original draft: Robert G. Hilton

Writing – review & editing: Robert G. Hilton, Jens M. Turowski, Matthew Winnick, Mathieu Dellinger, Patrick Schleppi, Kenneth H. Williams, Corey R. Lawrence, Katharine Maher

megatons of carbon per year, MtC yr^{-1} (Petsch, 2013). The process plays a central role in the geological carbon cycle (Derry & France-Lanord, 1996; Hayes et al., 1999; Hilton & West, 2020), and in part, governs oxygen concentrations in the atmosphere (Berner & Canfield, 1989).

To quantify the CO_2 emissions from OC_{petro} oxidation and understand the controls on these fluxes in modern-day catchments, several approaches have been considered. First, the residue of chemical weathering reactions can be traced across a weathering profile (Longbottom & Hockaday, 2019; Petsch et al., 2000; Wildaman et al., 2004). This can help understand the mechanisms that control OC_{petro} oxidation, such as the role of microbial communities (e.g., Hemingway et al., 2018). However, rates of weathering are difficult to quantify from weathering profiles, and measurements are inherently made at a local scale. Second, the production of CO_2 from rock weathering can be tracked in the weathering zone, but measurements have been limited to a handful of sites (Keller & Bacon, 1998; Soulet et al., 2018, 2021; Tune et al., 2020). A third approach uses the residue of weathering reactions carried by the sediment loads of rivers (Bouchez et al., 2010; Hilton et al., 2011). This provides a larger-scale view and has provided an insight in large rivers transiting floodplains where weathering intensity can be high (Galy et al., 2008; Lupker et al., 2011). However, when the erosion rates of OC_{petro} are high and the weathering intensity is lower, for instance in mountain river catchments, the sediment load may not resolve weathering losses (Hilton et al., 2011; Scheingross et al., 2019). An alternative approach is to use redox sensitive elements, such as rhenium, whose behavior makes them suitable as a proxy for OC_{petro} oxidation (Dalai et al., 2002; Hilton et al., 2014; Jaffe et al., 2002).

The element rhenium (Re, atomic weight $186.207 \text{ g mol}^{-1}$, isotopes ^{185}Re and ^{187}Re) has been proposed to track and quantify OC_{petro} oxidation (Jaffe et al., 2002). The Re proxy is grounded on the observation that OC_{petro} and Re are associated in sedimentary rocks. In seawater, Re is present as an oxyanion, ReO_4^- (Colodner et al., 1993). Under reducing conditions within marine sediments, Re is reduced and becomes insoluble (Colodner et al., 1992; Crusius et al., 1996; Crusius & Thomson, 2003) and can be immobilized by association with organic matter and mineral surfaces, in analogy with other trace elements (Dustin et al., 2018). Rhenium can also be incorporated into organic matter (Cohen et al., 1999; Rooney et al., 2012; Selby & Creaser, 2003). When sedimentary rocks are exposed to oxygen in the atmosphere and hydrosphere, for example, by exhumation during mountain building, OC_{petro} loss has been shown to be coupled with Re loss from solids (Hilton et al., 2014; Horan et al., 2017; Jaffe et al., 2002). During oxidative weathering, Re is thought to reform the soluble oxyanion ReO_4^- (Brookins, 1986), which can enter soil pore waters, streams, and rivers (Colodner et al., 1993; Miller et al., 2011). Thus, the dissolved Re flux from a catchment can provide constraint on the oxidative weathering fluxes upstream (Dalai et al., 2002).

Dissolved Re concentrations in river water are typically of the order of picograms per gram (i.e., $10^{-12} \text{ g g}^{-1}$, or parts per trillion, ppt) (Miller et al., 2011). These concentrations may now be measured directly in a water sample by quadrupole inductively coupled plasma mass spectrometry (Q-ICP-MS), or high resolution (HR) ICP-MS using a range of calibration standards (Hilton et al., 2014; Miller et al., 2011; Scheingross et al., 2019), and/or by using isotope dilution (Horan et al., 2017, 2019). The main challenge for the use of the Re proxy of OC_{petro} oxidation is thus no longer analytical. Instead, difficulties remain with the interpretation of the measured concentrations, because Re could be sourced from a range of phases in rocks alongside OC_{petro} , such as silicate and sulfide minerals (Miller et al., 2011). The ratio of dissolved Re to other ions mobilized from silicate and sulfide weathering (e.g., $[\text{Na}^+]$, $[\text{SO}_4^{2-}]$) can tease apart these contributions (Dalai et al., 2002; Horan et al., 2019). Additional insight may come from examining the relationships between Re concentration and water discharge ($C\text{-}Q_w$ relationships) and dissolved rhenium-ion ratios and water discharge. Concentration-discharge relationships have been used to shed light on hydrological processes (e.g., Anderson et al., 1997) and their links to the sources and pathways of major ions and trace elements derived from silicate, carbonate, and sulfide mineral weathering in rivers (e.g., Baronas et al., 2017; Calmels et al., 2011; Ibarra et al., 2017; Maher, 2011; Tipper et al., 2006; Winnick et al., 2017). However, until now, only a couple of time series of dissolved Re have been measured (Miller et al., 2011), and the hydrological context of Re mobilization has not been assessed.

Here, we assess the mobility and source of Re during weathering by measuring dissolved Re concentration over an annual time series in a pair of catchments in the pre-Alps of Switzerland, the Erlenbach and Vogelbach (Keller & Weibel, 1991; Schleppi et al., 2006), and in the East River in the Colorado Rockies (Hubbard et al., 2018; Winnick et al., 2017; Zhi et al., 2019). The three catchments drain sedimentary rocks. Dissolved

Re concentrations, fluxes, and ion ratios ($[\text{Re}]/[\text{Na}^+]$, $[\text{Re}]/[\text{SO}_4^{2-}]$) are used to explore the source of Re and how it may change with water discharge. Based on measurements from the three alpine catchments, we propose a conceptual model to link hydrological flow pathways to the mobilization of Re from the weathering zone. The findings are discussed in the context of the application of Re as a proxy of OC_{petro} oxidation.

2. Materials and Methods

2.1. Study Locations

2.1.1. Swiss Pre-Alps—Erlenbach and Vogelbach

The Erlenbach (drainage area = 0.74 km²) and Vogelbach (1.58 km²) catchments are located in the Alptal valley of the Swiss pre-Alps and monitored by the Swiss Federal Institute for Forest, Snow and Landscape Research—WSL (Hegg et al., 2006; Von Freyberg et al., 2018) for water discharge (Q_w , L s⁻¹), suspended sediment concentration (mg L⁻¹), suspended sediment and bedload yields (t km⁻² yr⁻¹), and sediment transport processes (Rickenmann et al., 2012; Keller & Weibel, 1991; Rickenmann & McARDell, 2007; Turowski et al., 2011, 2013). They have also been monitored for dissolved fluxes associated with ions, nutrients, and dissolved organic carbon (Hagedorn et al., 2000; Schleppi et al., 1998, 2006), which have been interpreted in terms of hydrological sources and pathways (Knapp et al., 2020; Von Freyberg et al., 2018). The “young water fraction” has been quantified for a range of flows, defined by Von Freyberg et al. (2018) as the proportion of catchment outflow younger than approximately 2–3 months. In an assessment of 22 Swiss catchments, the Erlenbach and Vogelbach have high “young water fractions,” whose values increase with water discharge (Von Freyberg et al., 2018), suggesting broadly similar hydrological conditions act in these catchments. The Erlenbach has also been sampled to constrain particulate OC source and flux (Smith et al., 2013; Turowski et al., 2016), allowing us to place oxidative weathering in the context of other carbon transfers.

The Swiss catchments share broadly similar climate, land cover types, and sedimentary rock lithology (Hegg et al., 2006), but have contrasting physical erosion rates (Keller & Weibel, 1991). The Erlenbach and Vogelbach have a mean annual precipitation (1987–2009) of 2,294 mm yr⁻¹ and 2,159 mm yr⁻¹, respectively (WSL, 2019), with ~30% falling as snow in the winter months. The mean annual runoff (1987–2009) is 1,778 mm yr⁻¹ and 1,601 mm yr⁻¹, respectively (WSL, 2019). However, the mean annual sediment yields (1986–1989) were 1,225 t km⁻² yr⁻¹ for the Erlenbach and 725 t km⁻² yr⁻¹ for the Vogelbach (Keller & Weibel, 1991). More recent sediment yield estimates are available for the Erlenbach of 1,648 t km⁻² yr⁻¹ from 1983 to 2011 (Smith et al., 2013), but not the Vogelbach. The Erlenbach is underlain by pelitic turbidites of Eocene age, which are part of the Wägital-Flysch Formation (Winkler et al., 1985). These rocks are similar to those found in the Vogelbach, but the Erlenbach has a cover of glacial till in the lower parts of the catchment (Hegg et al., 2006) that supplies fine-grained sediment and contributes to the sediment yield, in addition to erosion of the mudstone bedrocks (Schuerch et al., 2006; Smith et al., 2013).

Previous work has measured the OC concentration of rocks following carbonate removal (HCl leach) and analysis by Elemental Analyzer (Smith et al., 2013), with rocks from the Erlenbach having a mean OC content of $0.54 \pm 0.11\%$ ($n = 22$), similar to rock from the Vogelbach that range from 0.10% to 0.76% ($n = 4$) (Smith et al., 2013). River suspended sediments carry a mixture of OC eroded from vegetation, soil, and rock, as revealed by their carbon and nitrogen isotopic composition; this reflects the erosion processes, which deliver fine sediments to the channel via shallow landsliding, creep, particle abrasion, and bedrock incision (Schuerch et al., 2006; Smith et al., 2013). The export of solid load OC_{petro} from the Erlenbach catchment has been estimated using radiocarbon and stable C and N isotope ratios of organic matter to partition sources, and concentration-discharge relationships to quantify a flux of unweathered OC_{petro} of 10.1 ± 1.6 tC km⁻² yr⁻¹ (Smith et al., 2013).

2.1.2. Colorado Rockies—East River

The upper East River catchment (84 km²) is an important headwater source for the Gunnison and Colorado Rivers in the USA (Ugland et al., 1986) and has been instrumented as part of the Lawrence Berkeley National Laboratory's Watershed Function Scientific Focus Area (Carroll et al., 2018; Winnick et al., 2017). Recent work has established the behavior of major solutes as a function of the hydrological regime (Carroll et al., 2018; Winnick et al., 2017) and identified sulfide reaction fronts in the subsurface (Wan et al., 2019).

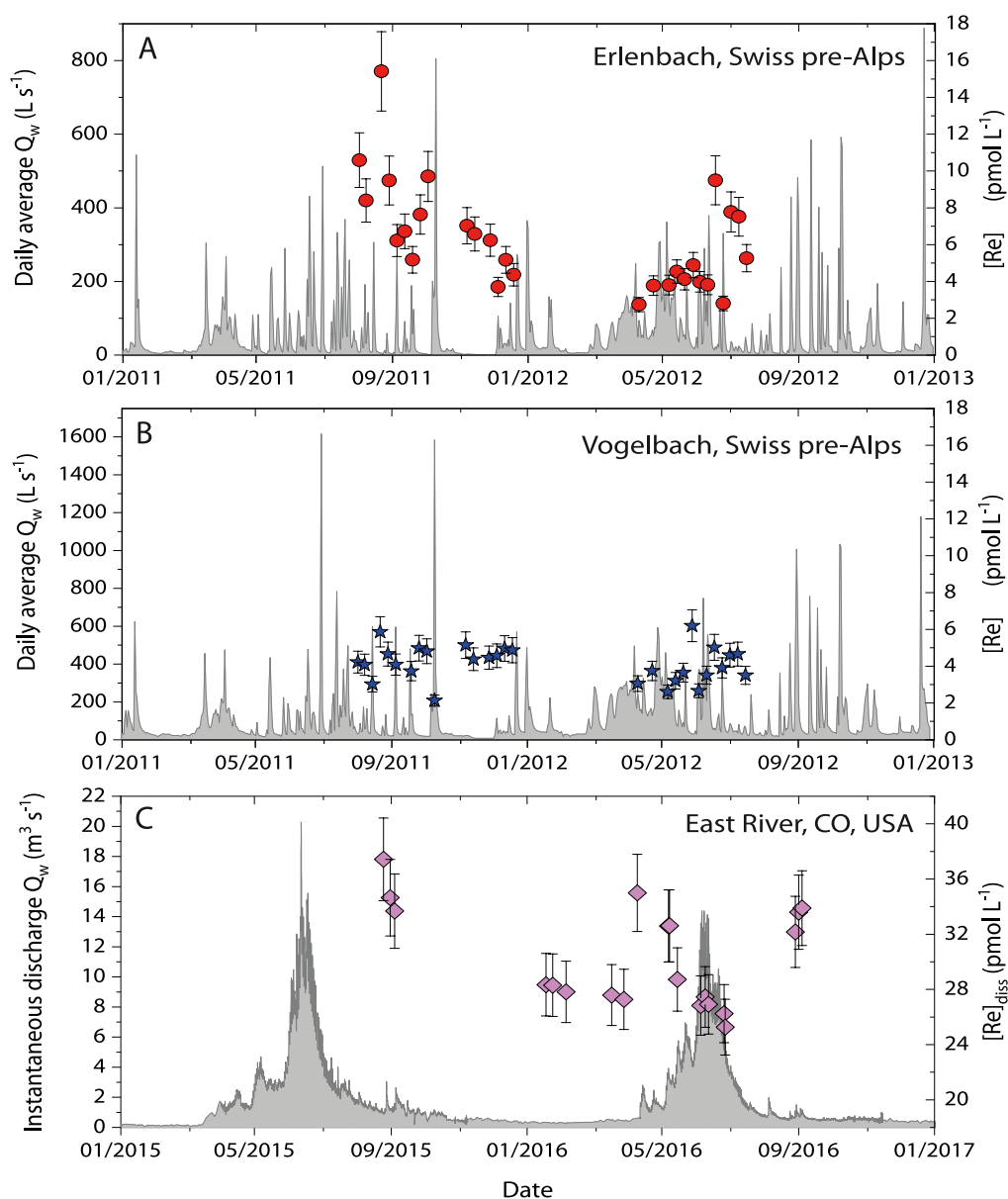


Figure 1. Samples collected for this study from the: (a) Erlenbach, Switzerland; (b) Vogelbach, Switzerland; and (c) the East River, Colorado, USA. In all panels, water discharge record is shown in gray and the symbols show measured dissolved rhenium concentration, $[Re]$ $pmol L^{-1}$, with whiskers showing the analytical uncertainty.

The East River catchment is much larger than the Swiss catchments, and the other main contrast is the general pattern of the annual hydrograph (Figure 1). The water discharge displays less short-term variability, and the signal is dominated by snowmelt, punctuated by summer monsoon events.

The mean annual precipitation for proximal weather stations over the past 30 years is $1230 mm yr^{-1}$, with the majority occurring as snowfall owing to the high elevation of the catchment (mean = 3,350 m) and mean annual temperature of $1^{\circ}C$ (PRISM, 2013). The catchment is primarily underlain by shale bedrock as part of the Mancos Shale of Late Cretaceous age (Morrison et al., 2012; Wan et al., 2019), with outcrops of Miocene quartz monzonite and granodiorite along with Paleozoic and Mesozoic sandstones. In the floodplains and lower slopes, alluvial and glacial deposits are present (Gaskill et al., 1967). The shales are rich in carbonate (20%), sulfide minerals (1%), and organic matter ($\sim 1\%$) (Morrison et al., 2012; Wan et al., 2019). Recent work has highlighted the important role of oxidation of sulfides on acid-production, carbon cycling,

and river water chemistry (Winnick et al., 2017). This suggests that the source of SO_4^{2-} from primary evaporite minerals in the Mancos Shale is negligible, and SO_4^{2-} derives primarily from pyrite oxidation. The shales are subjected to oxidative weathering (Wan et al., 2019; Winnick et al., 2017), but the erosion rate is fast enough that a fraction is exported from the catchment and cascades through the river system as OC_{petro} in the solid load (Fox et al., 2020).

2.2. Sample Collection and Preparation

In the Erlenbach and Vogelbach catchments, river water samples were collected weekly by hand, lowering a 1L bottle into the channel just above the gauging station installation, between 02/08/2011 and 16/07/2012 (Figures 1a and 1b, Table S1 in Supporting Information S1). A total of 29 samples were collected from the Erlenbach and 30 from the Vogelbach. River water samples were filtered through an acid-cleaned Nalgene vacuum filtration tower operated by a hand pump. Nylon filters of 0.2 μm pore and 47 mm diameter were used and filtered water was collected into pre-acid-cleaned bottles. An aliquot of ~ 250 ml was collected for major cations and trace elements and acidified to pH ~ 2 with trace analysis grade HNO_3 . Approximately 60 ml were collected for anion analysis in an unacidified aliquot. Two samples of snow were collected in April 2012 (Table S1 in Data Set S1) and rocks and river bed materials were obtained following a previous study (Smith et al., 2013). As part of the WSL observatory, cation and anion concentrations were also determined on samples collected using an autosampler from the river from 2005 to 2016.

In the East River, water samples for this study were collected from August 2015 to September 2016 using an automatic water sampler (Model 3700; Teledyne ISCO, NE, USA) using methods described previously (Winnick et al., 2017). A peristaltic pump sampled water from the main stream into 1 L polyethylene bottles and was retrieved at regular intervals. Samples for cation and trace metals analysis were filtered using 0.45 μm Hydrophilic Polyvinylidene Fluoride (PVDF) syringe filters into individual vials and acidified using concentrated trace metals grade nitric acid (Figure 1c).

Samples from a profile through sub-surface soil into weathered rock were collected in 2019 from the East River catchment at the Bradley Creek Meadow site (BM samples in Table S6 in Data Set S1), a subalpine meadow located at 2,987 m elevation. These comprised of seven samples collected from the surface to 1 m. The Bradley Creek Meadow site has been a focus of previous work (Hsu et al., 2018), with the BM samples collected within 3 m of the profile BC6 reported in Hsu et al. (2018), for which we also present new geochemical data.

2.3. Analytical Procedures

The concentration of dissolved Re, $[\text{Re}]$ pmol L^{-1} , was determined on filtered river water samples from the Erlenbach and Vogelbach by High Resolution ICP-MS (Thermo Fisher Scientific Element™) in Durham University. For the East River, $[\text{Re}]$ was measured by Q-ICP-MS (Agilent) in the Department of Geography, Durham University (Sproson et al., 2018), alongside a subset of samples from the Erlenbach and Vogelbach Rivers. A set of Re standards of varying concentrations from 0.1 to 20 ppt were used and instrumental drift accounted for by the use of sample doping with internal standards (Q-ICP-MS) and by the use of non-calibrating internal standards dispersed through a run (HR-ICP-MS). During the run, SLRS-5 and SLRS-6 standards were analyzed (undiluted and diluted by a factor of 10 and 100). For this study, the within run analysis of the river water standard SLRS-5 returned a value of 58.9 ppt (Q-ICP-MS), which is within the range of an inter-laboratory calibration study of 66 ± 12 ppt (Yeghicheyan et al., 2013) and similar to that determined by isotope dilution at Durham University of 59.8 ± 1.7 ppt (Horan et al., 2017). The accuracy and precision of Q-ICP-MS measurements are better than 8%. The relative average error of sample duplicates by HR-ICP-MS was 7%, and the difference between the Q-ICP-MS and HR-ICP-MS analysis methods was 14% across 13 sample analyses (with no systematic positive or negative bias). Therefore, the HR-ICP-MS measurements on the Erlenbach and Vogelbach have a slightly lower accuracy, but the range of observed $[\text{Re}]$ values is much larger than this uncertainty (e.g., ~ 0.51 –2.9 ppt).

For the Swiss Rivers, major cations and ions were determined by ion chromatography and accuracy determined by the analysis of the LETHBRIDGE-03 standard. Major cation and anion concentrations in East River samples for the studied time interval have been previously presented (Carroll et al., 2018).

The Re concentration of solid samples from the Erlenbach and Vogelbach Rivers was determined on samples previously analyzed for organic carbon concentrations ([OC], %) and stable isotopic composition ($\delta^{13}\text{C}$, ‰) (Smith et al., 2013). Here, powdered samples were combined with a 50:50 mix of HF 27N and HNO_3 16N within PTFE beakers and heated at 120°C for at least 24 hr. To destroy fluorides, samples were evaporated to dryness at 80°C and then redissolved in aqua regia at 120°C for 24 hr. To destroy refractory organic matter, (OM), any residue was treated in 16M HNO_3 and aqua regia for several days at 160°C. Samples were evaporated to dryness and then redissolved in 1M HCl. To chemically separate Re from the sample matrix, we use columns with an inner diameter of 7.1 mm, filled with 1 mL of AG1-X8 resin (200–400 mesh) (Dellinger et al., 2020). The resin was first cleaned with 30 mL of 8M HNO_3 , and conditioned with 5 mL of 1M HCl. Samples were loaded at 1M HCl and the matrix removed in three steps (10 mL of 1M HCl, 15 mL of 0.5M HNO_3 , and 1.5 mL of 4M HNO_3) before elution of Re with 12.5 mL of 4M HNO_3 . The eluted Re fraction is then evaporated at a temperature of 100–120°C to complete dryness, retaken in 3% HNO_3 , and the concentration determined by Q-ICP-MS. A range of standard reference materials were treated to the same chemistry and had Re yields of 95.3% (Dellinger et al., 2020). Powdered solid samples from the BM profile of the East River were processed in the same way to determine their Re concentration.

The [TOC] concentration, %, of BM samples was determined by the difference of total carbon concentration (TC by combustion, %) and total inorganic carbon (TIC by acidification, %) via Analytik Jena EA4000, with accuracy and precision assessed to be 5% using a certified EURO SOIL standard (Table S6 in Data Set S1). For BC6, as reported in Hsu et al. (2018), total organic carbon concentrations, [TOC]%, were measured on sample splits following inorganic removal by elemental analyses with a Carlo-Erba NA 1500 analyzer (Thermo Fisher Scientific, Waltham, MA, USA) and major element geochemistry via XRF, at the Environmental Measurements Facility (EM1) of Stanford University, Stanford, CA, USA. In addition, we present new radiocarbon activity measurements (reported as Fraction Modern, $F^{14}\text{C}$) on bulk organic matter from a neighboring profile BC6 (Table S6 in Data Set S1). For radiocarbon analysis, separate sample aliquots were sent to the U.S. Geological Survey (USGS) ^{14}C Laboratory in Reston, VA, USA for processing and sample preparation. At the USGS laboratory, carbonates were removed from the bulk sample by acid-rinsing and a sub-split was analyzed for $\delta^{13}\text{C}$ by an isotope ratio mass spectrometer. The remainder of the sample was then combusted to CO_2 , which was then purified and converted to graphite targets. The graphite targets were then sent to the Lawrence Livermore National Laboratory Center for Accelerator Mass Spectrometry (LLNL-CAMS) in Livermore, CA, USA where the radiocarbon content was determined by AMS and reported as Fraction Modern, $F^{14}\text{C}$ (Reimer et al., 2004).

2.4. Dissolved Flux Calculations

The relationships between water discharge and ion concentrations provide an insight on ion source and weathering reactions (Godsey et al., 2009; Knapp et al., 2020; Tipper et al., 2006; Winnick et al., 2017) and constrain dissolved ion fluxes (Schleppi et al., 2006). For the Erlenbach and Vogelbach catchments, which were sampled at the same frequency (Figures 1a and 1b), we explore a rating curve approach to quantify dissolved yields, by fitting power law functions to concentration-discharge data (Figure 2). Ion concentrations are then predicted for each daily discharge value using these functions, and annual fluxes determined by summing daily values. To quantify the uncertainty on the total ion fluxes, we run a Monte Carlo simulation for which each daily concentration value is allowed to vary between the 2SE bounds of the power law fit (a full probability distribution) and run 10,000 iterations of the sum of the total annual ion flux. We also quantify dissolved Re flux using the water discharge-weighted average [Re] concentration for all three basins.

3. Results

3.1. Swiss Pre-Alps—Erlenbach and Vogelbach

3.1.1. Dissolved Load

In both the Erlenbach and Vogelbach catchments, dissolved Ca^{2+} concentrations are negatively correlated with runoff (Q_w normalized to catchment area, $\text{L km}^{-2} \text{s}^{-1}$) (Figure 2a) and can be described by power law fits to the data (Table S2 in Data Set S1). These support findings from previous work in the Erlenbach catchment (Knapp et al., 2020; Schleppi et al., 2006). The 2011–2012 samples are similar to the 2005–2016 WSL

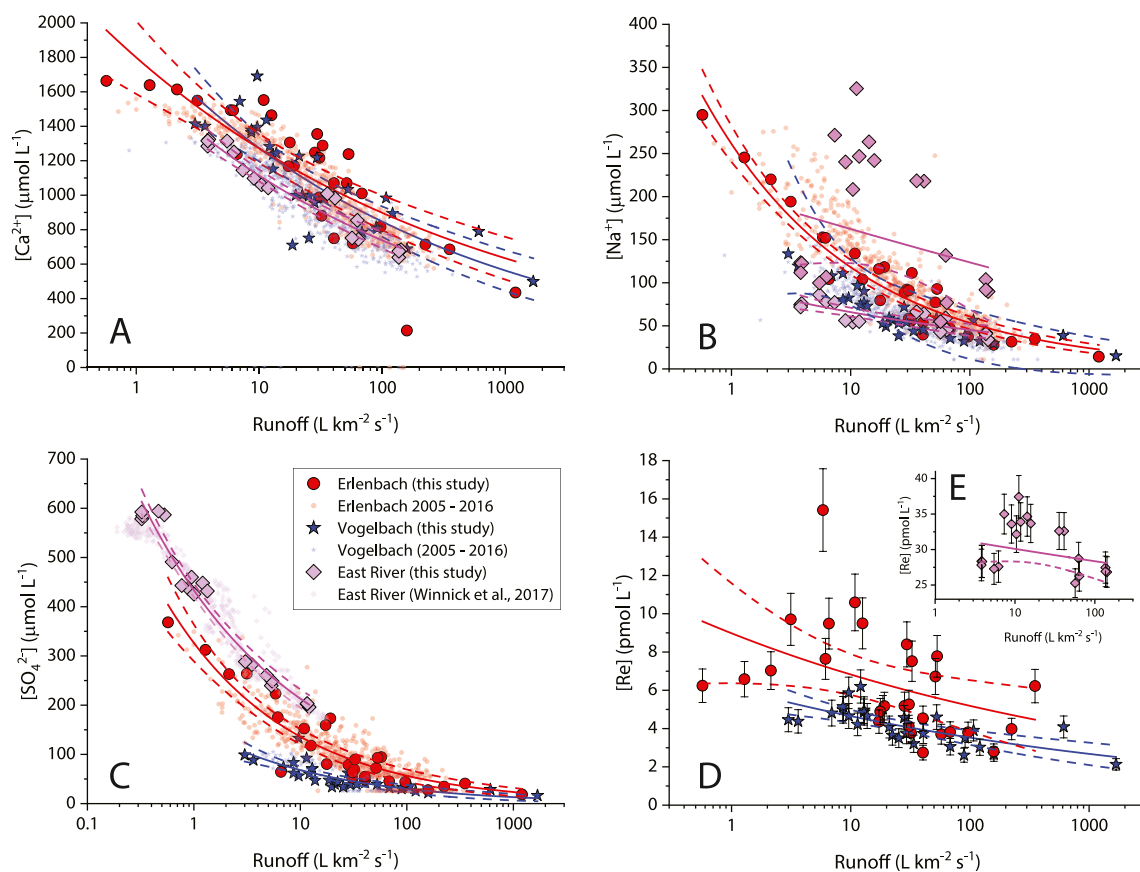


Figure 2. Instantaneous runoff (water discharge normalised by drainage area) versus dissolved concentrations of: (a) calcium $[Ca^{2+}]$, $\mu\text{mol L}^{-1}$; (b) sodium $[Na^+]$, $\mu\text{mol L}^{-1}$; (c) sulfate $[SO_4^{2-}]$, $\mu\text{mol L}^{-1}$; and (d) rhenium $[Re]$, pmol L^{-1} , with (e) $[Re]$ from the East River (note change in axis scale). Data from this study (2011–2012) are shown as large symbols for the Erlenbach (red circles), Vogelbach (blue stars), and East River (pink diamonds) with whiskers showing the analytical uncertainty (if larger than the point size). Power law fits to the data (lines) with their 95% confidence intervals (dashed lines) are shown (see Table S2 in Data Set S1 for fitting parameters and r^2 values). In panels, smaller symbols are a longer time series of data from the WSL observatory from 2005–2016 for the Erlenbach and Vogelbach, and data from the East River from Winnick et al. (2017).

data, but cover a slightly wider range of runoff values (Figure 2a). This reflects the flow-weighted sampling methods applied to collect and process the WSL data (Schleppi et al., 2006), whereas our sample design has captured more high flow events. Other major cations, such as Na^+ (Figure 2b) and Mg^{2+} have a similar C- Q_w behavior between catchments (Table S2 in Data Set S1). However, the concentrations of SO_4^{2-} are different between the catchments (Figure 2c). Both rivers show negative correlations with runoff, which can be described by power law fits, $[X] = a \times \text{Runoff}^b$, where $[X]$ is the ion concentration and a and b are constants (Table S2 in Data Set S1). The Erlenbach has higher SO_4^{2-} concentrations, particularly at lower runoff values (Figure 2c).

Dissolved Re concentrations in the Erlenbach had a mean $[Re] = 6.3 \pm 2.8 \text{ pmol L}^{-1}$ ($n = 28$, \pm standard deviation, unless otherwise stated from here) and a range from 2.7 to 15.4 pmol L^{-1} (Table S1 in Data Set S1). The water discharge-weighted average dissolved $[Re]$ was 5.1 pmol L^{-1} . These concentrations are similar to other rivers draining sedimentary rocks (Hilton et al., 2014; Miller et al., 2011). In the Vogelbach, the mean $[Re] = 4.1 \pm 1.0 \text{ pmol L}^{-1}$ and varied from 2.13 to 6.20 pmol L^{-1} . Weighted by water discharge, the average dissolved $[Re]$ in the Vogelbach was 2.9 pmol L^{-1} . The two snow samples collected in April 2012 had very low Re concentrations (below detection limit by HR-ICP-MS in this study, of $<0.1 \text{ pmol L}^{-1}$), similar to Re in rainwater from New Zealand (Horan et al., 2017), but in contrast with higher Re concentrations in rainwater near industrial sources (Miller et al., 2011).

Both catchments have a broad negative relationship between $[Re]$ and runoff (Figure 2d) (Table S2 in Data Set S1), but with the Erlenbach having higher $[Re]$ values, particularly at low to intermediate runoff values.

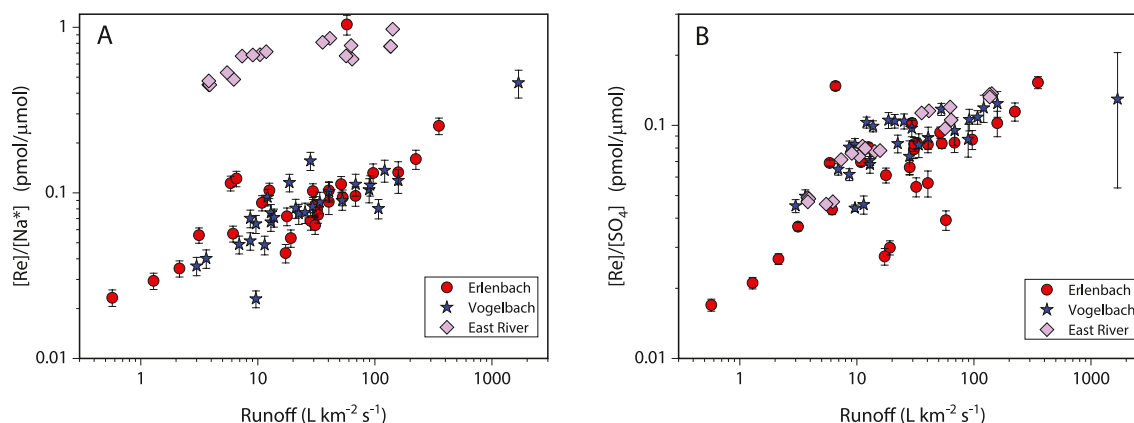


Figure 3. Instantaneous runoff (water discharge normalised by drainage area) versus dissolved: (a) rhenium to sodium ratio, $[\text{Re}]/[\text{Na}^+]$ pmol/ μmol and (b) rhenium to sulfate ratio, $[\text{Re}]/[\text{SO}_4^{2-}]$ pmol/ μmol . Data are shown for the Erlenbach (red circles), Vogelbach (blue stars), and East River (pink diamonds), with whiskers showing the analytical uncertainty (if larger than the point size).

The relationship can be fit by a power law (Table S2 in Data Set S1), but the fit is poor for the Erlenbach (Figure 2d, Table S2 in Data Set S1). Although the data set is limited in length, there is some suggestion of seasonality in $[\text{Re}]$ values in the Erlenbach, with the highest concentrations measured in July and August (Figure 1a).

The ratios of dissolved Re with Na^+ and SO_4^{2-} have been proposed as tools to help examine the source of dissolved Re in river water (Horan et al., 2019). Here, we correct Na^+ concentrations for atmospheric-derived Na, $[\text{Na}^+]$, where $[\text{Na}^+]^* = [\text{Na}^+] - [\text{Cl}^-] \times 0.85$, assuming all Cl^- derives from precipitation, which has a molar $[\text{Na}^+]/[\text{Cl}^-]$ ratio of 0.85. Despite the differences in $[\text{Re}]$ between the Erlenbach and Vogelbach Rivers (Figure 2d), the very similar ion ratios show positive correlations between runoff and $[\text{Re}]/[\text{SO}_4^{2-}]$ and $[\text{Re}]/[\text{Na}^+]$ values (Figure 3). The $[\text{SO}_4^{2-}]$ concentrations may include a source of sulfate from atmospheric deposition, which has decreased dramatically in recent decades but is still an important source of sulfate in the catchments (Thimonier et al., 2005).

3.1.2. Dissolved Flux

Over 2011–2012 water years, the average annual runoff for the Vogelbach was slightly lower (2,249 mm yr^{-1}) than the Erlenbach (2,451 mm yr^{-1}), with the ratio Erlenbach:Vogelbach = 1.1 (Table S3 in Data Set S1). We find Ca^{2+} and Mg^{2+} fluxes, which have a ratio of Erlenbach:Vogelbach of 1.1 and 1.2, respectively, which is very similar to the contrast in runoff over the sampling period. In contrast, the SO_4^{2-} and dissolved Re fluxes are elevated in the Erlenbach, with an Erlenbach:Vogelbach flux ratio of 1.8 and 1.6, respectively.

The 2011–2012 calculated dissolved Re yields, based on the power law fits to concentration-discharge relationships, were $1.24^{+0.05}_{-0.04} \times 10^{-2} \text{ mol km}^{-2} \text{ yr}^{-1}$ and $0.79^{+0.01}_{-0.01} \times 10^{-2} \text{ mol km}^{-2} \text{ yr}^{-1}$ for the Erlenbach and Vogelbach, respectively. However, the power law fit between $[\text{Re}]$ and runoff was poor for the Erlenbach (Figure 2c, Table S2 in Data Set S1) and did not fully capture variability with flow. As such, we also estimate the dissolved Re yield using an alternative method. Using water discharge weighted average $[\text{Re}]$ and the mean discharge for the sampling period for the Erlenbach (5.1 pmol L^{-1} , and 5.7 L s^{-1}) and Vogelbach (2.9 pmol L^{-1} ; and 112 L s^{-1}), we return a dissolved Re yield of $1.2 \times 10^{-2} \text{ mol km}^{-2} \text{ yr}^{-1}$ for the Erlenbach, and $0.66 \times 10^{-2} \text{ mol km}^{-2} \text{ yr}^{-1}$ for the Vogelbach. The two methods to calculate dissolved flux return similar values within ~20%.

3.1.3. Solid Materials

The Re concentration in rocks, $[\text{Re}]_{\text{rock}}$, varied from 0.58 to 9.74 ppb and were broadly, positively correlated with the organic carbon concentration, $[\text{OC}]$ ($r = 0.68$, $P = 0.06$, $n = 8$). Excluding the highest concentration sample, the mean $[\text{Re}]_{\text{rock}} = 1.16 \pm 0.48 \text{ ppb}$ ($n = 7$) (Table S4 in Data Set S1). The mean $[\text{Re}]_{\text{rock}}/[\text{OC}]$ ratios were $3.3 \pm 2.5 \times 10^{-7} \text{ g g}^{-1}$ ($n = 8$) with a range from 1.75×10^{-7} to $8.93 \times 10^{-7} \text{ g g}^{-1}$. These $[\text{Re}]_{\text{rock}}$ concentrations and $[\text{Re}]_{\text{rock}}/[\text{OC}]$ ratios are similar to those measured in gray shales and sedimentary rocks elsewhere (Dalai et al., 2002; Hilton et al., 2014; Horan et al., 2017).

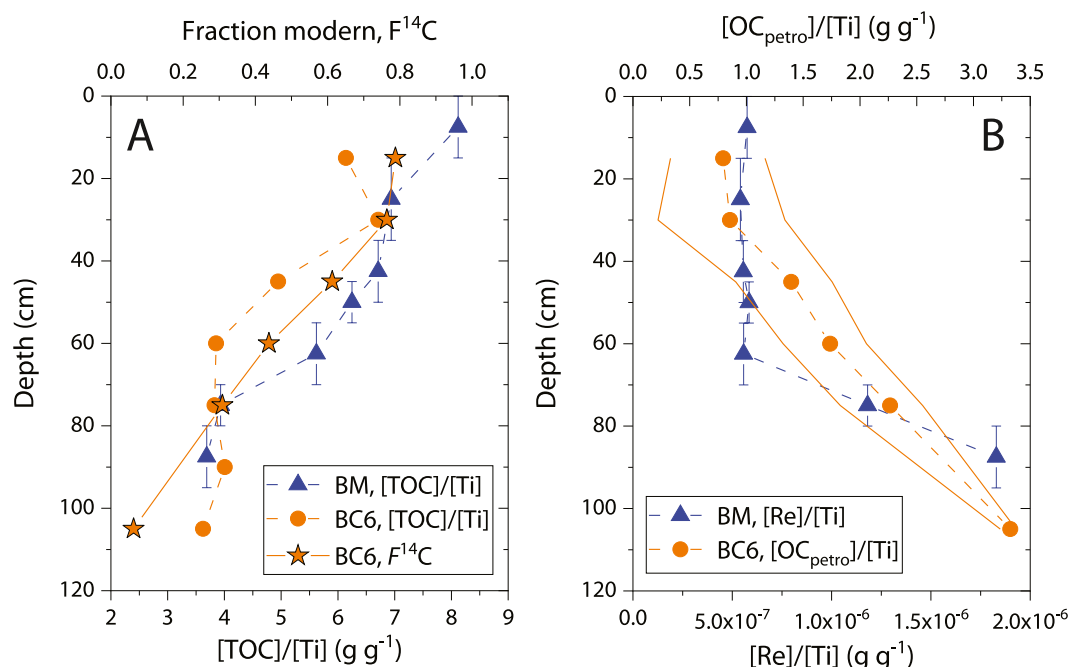


Figure 4. Weathering profiles from Bradley Creek Meadows. The two profiles BM and BC.6 were collected with ~ 3 m of each other. (a) Total organic carbon concentration ($[TOC]$) normalized to titanium ($[Ti]$) from site BM (blue triangles this study) and site BC.6 (orange circles, Hsu et al., 2018), with radiocarbon measurements from BC.6 (orange stars, this study) reported as the Fraction Modern, $F^{14}C$. (b) Rhenium concentration ($[Re]$, ppb) for site BM (black circles) and modeled rock organic carbon concentrations ($[OC_{petro}]$, %) from site BC.6 (blue squares and blue lines showing $\pm 1\sigma$ range) that derive from $[TOC]$ and $F^{14}C$ (Table S6 in Data Set S1).

3.2. East River, Colorado Rockies

3.2.1. Dissolved Load

The 2015–2016 samples analyzed here for $[Re]$ have similar major ion chemistry to the samples reported by Winnick et al. (2017) from 2014–2015 (Figure 2). In summary, the concentrations of Ca^{2+} has similar trends with Q_w . Sulfate has a more pronounced dilution. Dissolved Re concentrations in the East River had a mean $[Re] = 30.3 \pm 3.6\ \text{pmol}\ L^{-1}$ ($n = 20$) with a range from 25.3 to 37.4 $\text{pmol}\ L^{-1}$ (Table S5 in Data Set S1). The water-discharge weighted average $[Re]$ was 28.3 $\text{pmol}\ L^{-1}$. These concentrations are more than double the estimated global mean $[Re]$ (Miller et al., 2011) but similar to rivers in the Mackenzie River Basin, where OC-rich sedimentary rocks are widespread (Horan et al., 2019). There was a broad negative correlation between $[Re]$ and runoff ($r = -0.48$, $P = 0.03$) (Figure 2d) and some suggestion of temporal hysteresis in the data set associated with snowmelt (Figure 1c), that is also seen in Na^+ concentrations, and so these data were not well described by a power law trend ($R^2 = 0.04$).

The East River had similar $[Re]/[SO_4^{2-}]$ values when compared to the Vogelbach and Erlenbach, but higher $[Re]/[Na^+]$ ratios (Figure 3). Both the $[Re]/[SO_4^{2-}]$ and $[Re]/[Na^+]$ ratios are positively correlated with runoff in the East River, similar to the trends observed in the Swiss streams (Figure 3).

To provide a first-order estimate of dissolved Re flux by the East River, the water-discharge weighted average $[Re]$ was combined with the average discharge over the sampling period (28.3 $\text{pmol}\ L^{-1}$ and $2.5\ \text{m}^3\ s^{-1}$) to return a dissolved Re yield of $2.7 \times 10^{-2}\ \text{mol}\ km^{-2}\ yr^{-1}$ over the catchment area.

3.2.2. Solid Materials

In the weathering profile samples from Bradley Creek Meadow (BM), $[Re]$ concentration ranged from 2.02 to 6.42 ppb (Table S6 in Data Set S1). In the upper 70 cm of the profile, $[Re]$ was relatively constant with an average of 2.10 ± 0.06 ($n = 5$), before increasing to 4.38 ppb between 70 and 80 cm, and reaching 6.42 ppb at between 80 and 95 cm depth (Figure 4b). For comparison, the $[Re]$ of a sample of shale from the proximal

(<1 km) Rustler Gulch had a $[Re] = 20.31$ ppb. Whether this shale rock sample is representative of the unweathered rock beneath the BM site is not known. The higher $[Re]$ concentrations in the deeper BM profile may explain the higher dissolved $[Re]$ in the East River than when compared to the Swiss catchments and other global rivers. The $[Re]$ have been normalized to Ti to account for potential volume changes during pedogenesis (Figure 4).

The pattern in $[Re]/[Ti]$ with depth can be compared to the nearby BC6 soil profile, with newly measured radiocarbon activity, $F^{14}C$, alongside published $[TOC]$, %, and major element data (Figure 4a) (Hsu et al., 2018). The $F^{14}C$ in the deepest part of the profile at 105 cm is very low, with a value of 0.0629 ± 0.0006 . This could be explained by the input of ^{14}C -depleted OC_{petro} . Higher in the profile, $F^{14}C$ values increase, but remain somewhat ^{14}C -depleted even near the surface, with a $F^{14}C = 0.7879 \pm 0.0025$ at 15 cm depth.

We use the $F^{14}C$ values to estimate the potential contribution from OC_{petro} by considering its mixture with biospheric organic carbon:

$$F^{14}C \times [TOC] = F^{14}C_{petro} \times [OC]_{petro} + F^{14}C_{bio} \times [OC]_{bio} \quad (1)$$

where $F^{14}C$ and $[TOC]$ are the measured radiocarbon activity and organic carbon concentration of the sample, and the 'petro' and 'bio' subscripts refer to the rock organic carbon and more recent organic matter from the terrestrial biosphere, respectively. If we assume that the geological OC_{petro} is ^{14}C -depleted below background ($F^{14}C = 0$), and $[TOC] = [OC]_{petro} + [OC]_{biosphere}$, then:

$$[OC]_{petro} = [OC] \times \left(1 - \frac{F^{14}C}{F^{14}C_{bio}} \right) \quad (2)$$

The value of $F^{14}C_{bio}$ is uncertain, and should vary as the atmospheric bomb-spike is depleted and the organic matter in soil ages. However, it could range between ~ 1 and ~ 0.5 in a soil of 1 m depth based on a global data compilation (Lawrence et al., 2020). To estimate $[OC_{petro}]$, we therefore use a range of $F^{14}C_{bio}$ between 1.0 and 0.85 at the surface, and between 1.0 and 0.5 at depth (see Table S6 in Data Set S1), and assess uncertainty using a Monte Carlo simulation (MCSim Add-in Excel, with 1000 repetitions per sample across a full probability distribution, reporting the median and 1 sigma range). The modeled $[OC]_{petro} = 0.99 \pm 0.02\%$ at 105 cm depth, which decreases to $[OC]_{petro} = 0.34 \pm 0.11\%$ near the surface (BC.6.15) (Table S6 in Data Set S1). We note that the sulfur concentration of these samples is very low ($<0.04\%$) across the entire depth profile (Hsu et al., 2018).

While the OC and Re measurements were made on different profiles, they both show a decrease in both $[Re]/[Ti]$ and $[OC_{petro}]/[Ti]$ above ~ 60 – 75 cm depth (Figure 4b). The depletion is not due to dilution by recent organic matter because the relatively insoluble element titanium (Ti) does not decrease near the surface. Using the deepest samples from BM for $[Re]$ and BC.6 for OC_{petro} , the $[Re]/[OC_{petro}]$ ratio is $6.4 \times 10^{-7} \text{ g g}^{-1}$.

4. Discussion

The Swiss catchments studied here contrast in their erosion rates (Table S2 in Data Set S1) and both differ from the East River in terms of the sedimentary bedrock (Morrison et al., 2012; Winkler et al., 1985) and hydro-climate (Schleppi et al., 2006; Winnick et al., 2017). Despite these contrasts, the three catchments display remarkably similar behavior in terms of the observed increase in $[Re]/[Na^+]$ and $[Re]/[SO_4^{2-}]$ ratios with water discharge (Figure 3). Here, we discuss these patterns, and go onto propose a conceptual model to account for shifts in Re source and its pathway through shale catchments.

4.1. Oxidative Weathering of OC_{petro} as a Source of Re

In the weathering profiles collected from the East River, the BM site shows Re depletion between ~ 45 and ~ 95 cm depth. At the nearby BC.6 profile (within ~ 3 m) the modeled OC_{petro} contents are more uncertain, particularly near the surface (Table S6 in Data Set S1), but the data suggest OC_{petro} loss between 45 to 105 cm depth (Figure 4b). Using $[Ti]$ to normalize the concentration data and account for any volume changes in

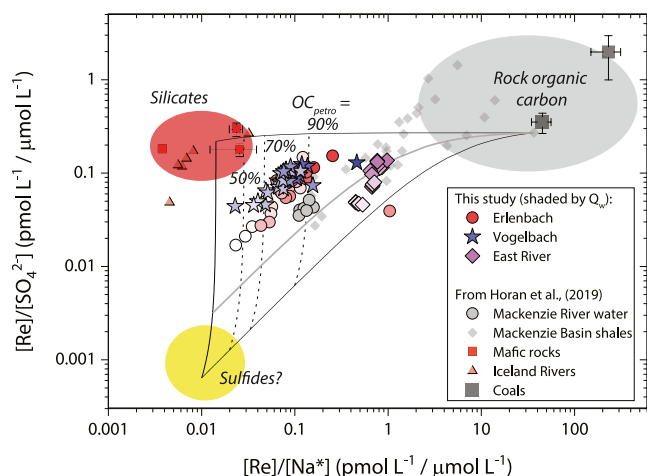


Figure 5. The rhenium to sodium, $[Re]/[Na]^+$, and rhenium to sulfate, $[Re]/[SO_4^{2-}]$, ratios ($\text{pmol } \mu\text{mol}^{-1}$) for river waters from this study (Erlenbach = red circles; Vogelbach = blue stars; and East River = pink diamonds), where the shading corresponds to low (clear) to high (colored) water discharge (Figure 3). The samples are shown in the context of a source mixing domain defined by Horan et al. (2019) between Re from rock organic carbon, sulfides, and silicate minerals, with Mackenzie Basin shales (Ross & Bustin, 2009), mafic rocks, Icelandic Rivers, and Coals as per Horan et al. (2019). Published data are also shown from the Mackenzie River main channel (gray circles) (Horan et al., 2019). Dashed lines are constant proportions of rock organic carbon-derived Re (90%, 70%, and 50%) and the gray line is a sulfide:silicate ratio of 0.2:0.8.

the materials as they weather, we find that between 95 and 45 cm the $[Re]/[Ti]$ decreased by $\sim 68\%$, while $[OC_{\text{petro}}]/[Ti]$ decreased by $\sim 59\%$. We note that the sulfur concentration in this soil profile is low ($<0.04\%$), and consistent throughout and the pyrite weathering front in this catchment is likely to lie deeper than the maximum depth sampled here (Wan et al., 2019, 2021; Winnick et al., 2017), marking a stark decoupling of Re from sulfides in this location. The loss of Re and $[OC_{\text{petro}}]$ from the near-surface weathering zone has been reported for a weathering profile on a black shale (Jaffe et al., 2002) and measurements of weathered materials from rocks with lower $[OC_{\text{petro}}]$ in Taiwan and New Zealand (Hilton et al., 2014; Horan et al., 2017). The coincidence of the zone of depletion of Re and OC_{petro} in the East River, and the similar degree of depletion, support the use of Re as a proxy to track OC_{petro} weathering.

To provide an independent constraint on Re source, we turn to river water where the ratios of the dissolved products of chemical weathering can be used (Gaillardet et al., 1999; Galy & France-Lanord, 1999). Here, we consider dissolved Re in the context of ions sourced from acid hydrolysis weathering of silicate minerals (e.g., Na^+) and oxidative weathering of sulfides (SO_4^{2-}) (Figure 5). Following the approach of Horan et al. (2019), a $[Re]/[Na]^+$ value of $\sim 0.01 \text{ pmol } \mu\text{mol}^{-1}$ could reflect silicate weathering and an Re source dominated by silicate minerals that are relatively Re depleted. Igneous rocks and Iceland Rivers draining basalt were used by Horan et al. (2019) to define the composition of a mafic rock endmember (Figure 5). For sulfide oxidation, a low $[Re]/[SO_4^{2-}]$ value of $\sim 0.001 \text{ pmol } \mu\text{mol}^{-1}$ has been proposed (Miller et al., 2011). The oxidation of OC_{petro} would thus supply Re with higher $[Re]/[Na]^+$ and $[Re]/[SO_4^{2-}]$ ratios. A set of shale bedrocks from the Mackenzie River Basin (Ross & Bustin, 2009) support this (Figure 5): their $[Re]/[Na]^+$ and $[Re]/[SO_4^{2-}]$

values decrease with increasing sulfur to organic carbon ratios, confirming that the sulfide source of Re has a low $[Re]/[SO_4^{2-}]$ (Horan et al., 2019).

The river water samples from the three Alpine catchments have $[Re]/[Na]^+$ and $[Re]/[SO_4^{2-}]$ values that can be explained by a mixture of weathering of sulfide, silicates, and OC_{petro} (Figure 5). Atmospheric inputs of SO_4^{2-} that have accumulated over time could provide additional input in the Swiss catchments (Thimoni-er et al., 2005) and this would act to lower the $[Re]/[SO_4^{2-}]$ values and shift the ratios away from the OC_{petro} end member. However, we note that the Erlenbach and Vogelbach have contrasting SO_4^{2-} concentrations and fluxes (elevated C- Q_w relationship for the Erlenbach—Figure 2b) despite their close proximity, with the more erosive catchment having a higher SO_4^{2-} flux (Table S3 in Data Set S1). This is indicative of a supply-limited reaction driving SO_4^{2-} supply, which has been observed for sulfide oxidation in other catchments (Calmels et al., 2007; Torres et al., 2016). Despite the contrast in dissolved SO_4^{2-} and Re fluxes, the Swiss catchments have similar ion ratios, which suggest a broadly similar Re source, with a higher silicate Re contribution than the East River (Figure 5). This could come about because of the higher [TOC] in the Mancos Shale (Morrison et al., 2012; Wan et al., 2019) compared to the Wagital flysch underlying the Vogelbach and Erlenbach (Smith et al., 2013). Overall, in the three basins the ion ratios are consistent with a mixing domain that suggests most dissolved Re comes from OC_{petro} , with the percentage of Re from OC_{petro} being $>70\%$ in the majority of the Swiss catchment samples.

4.2. Hydrological Constraints on Re Pathways of Mobilization

The $[Re]/[Na]^+$ and $[Re]/[SO_4^{2-}]$ ratios have been considered in terms of the weathering reactions occurring in the catchment, and the relative contributions of OC_{petro} , sulfide, and silicate minerals to the dissolved ion loads (Figure 5). However, these ratios vary notably and increase with runoff in all catchments (Figure 3).

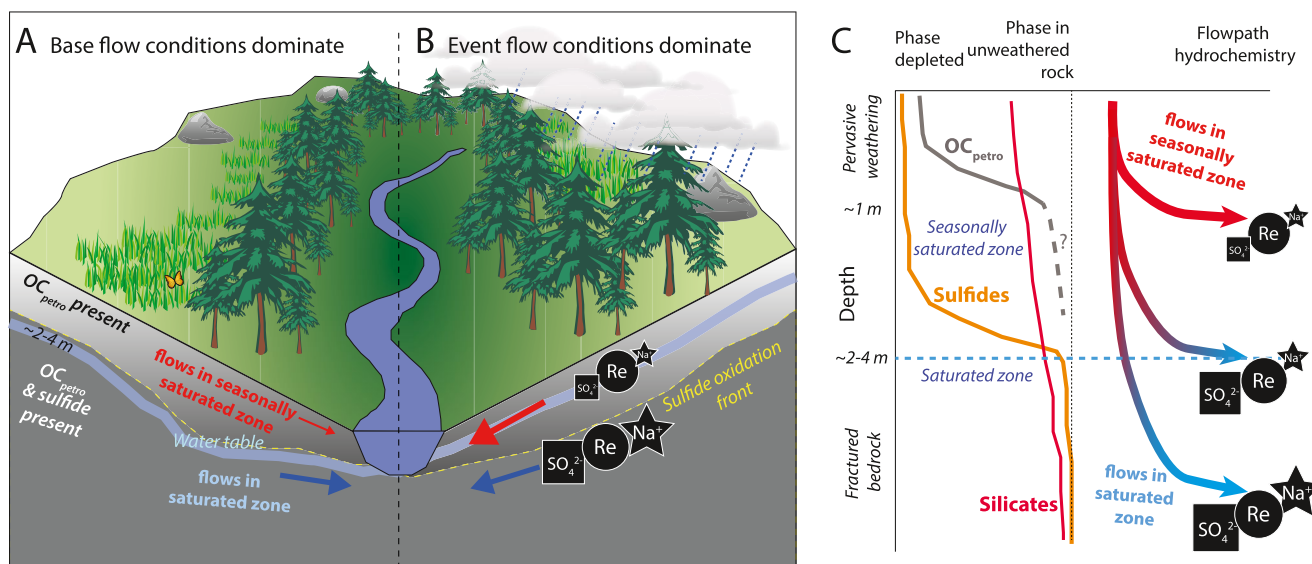


Figure 6. A conceptual model to explain the link between runoff, $[Re]/[Na^+]$ and $[Re]/[SO_4^{2-}]$ in the studied catchments (Figure 3). The cartoon shows a shale-dominated geology, with a sulfide oxidation front that has formed below the surface near the water table. Above the sulfide oxidation front negligible sulfide minerals remain, whereas rock organic carbon (OC_{petro}) is still found. (a) Under base flow conditions, flows through the saturated zone (blue arrows) can dominate the water budget over flows through the seasonally saturated zone (red arrows) comprising soil and saprolite. (b) During rainfall as water discharge increases, flows through the unsaturated zone increase in their relative importance. The dissolved ion concentration is indicated by the relative size of symbols (Re = circle, Na^+ = star, SO_4^{2-} = square). (c) A schematic view of the depletion of OC_{petro} (based on Figure 4), sulfides, and silicates (based on Wan et al., 2019, 2021) for the East River, with the conceptual model that explains the catchment hydrochemistry: Re is preferentially sourced from the unsaturated zone where OC_{petro} is present, SO_4^{2-} mobilized from the sulfide oxidative front, whereas enrichment in Na^+ requires longer flow pathways and/or greater fluid residence times.

Here, we discuss these patterns in the context of Re transport by different hydrological pathways, seeking to build a conceptual model to better understand Re mobilization during shale weathering (Figure 6).

The pathway and residence time of flowing water in catchments can impact the source and concentration of ions in streams and rivers (e.g., Barnes et al., 2018; Maher & Druhan, 2014; Maher et al., 2006). At low flow (or “base flow”), water in streams is generally considered to represent the pathways with the longest residence time (Anderson et al., 1997; Maher, 2011; McDonnell et al., 2010). Longer periods of interaction between water and soil or rock can increase the concentrations of elements derived from the slowest reacting minerals, as the fluid and solids approach chemical equilibrium (Maher et al., 2006). In contrast, during rainfall events, throughput of water by rapid and/or shallow flow pathways should have little time to interact with solids, and the fluids will be more dilute (Calmels et al., 2011; Hagedorn et al., 2000). The contrast between low and high flow is likely to be most pronounced for ions derived from minerals with weathering timescales that are comparable to subsurface residence times (Maher & Druhan, 2014).

In the Erlenbach and Vogelbach, Von Freyberg et al. (2018) quantified the “young water fraction,” the average fraction of flow that is younger than ~2–3 months (Kirchner, 2016), and find that it is correlated with water discharge. In the Erlenbach and Vogelbach, the lowest discharges have a young water fraction of ~0.3 and ~0.2, respectively (Von Freyberg et al., 2018), which suggests 70%–80% of the water has resided in the catchments for more than ~2–3 months. At high flow, the young water fraction reaches ~0.5 in the Erlenbach (Von Freyberg et al., 2018). A quantitative assessment has not been made for the East River, but a similar role of flow pathways and fluid residence time has invoked to explain the mobilization of solutes from carbonate, silicate, and sulfide mineral weathering (Winnick et al., 2017; Zhi et al., 2019). Overall, these contrasts in fluid residence times with water discharge can explain the observed increase in $[Re]/[Na^+]$ ratios with runoff in the catchments (Figure 3a). Base flow contributions become relatively enriched in Na^+ from silicate weathering, while higher discharges are dominated by younger waters that are relatively depleted in Na^+ (Figure 6b).

The changes in the relative concentrations of dissolved ions with discharge (Figure 3) can also reflect changes in mineral abundance and the location where reactions occur in the weathering zone (Figure 4). This is particularly the case for oxidative weathering reactions, because the availability of gaseous or dissolved oxygen and mineral phases for weathering is so important (Bolton et al., 2006). The formation of oxidative weathering fronts is a common observation, where sulfides and OC_{petro} show pronounced depletion near the surface where oxygen availability is greater (Brantley et al., 2013; Gu et al., 2020; Petsch, 2013; Wan et al., 2019; Wildman et al., 2004). The porous, unsaturated vadose zone can experience high rates of oxidative weathering (Soulet et al., 2018, 2021), while saturated conditions can quickly consume dissolved O_2 in porewaters where sulfide minerals are present and react quicker than OC_{petro} (Bolton et al., 2006). This can result in the formation of a deeper weathering front for sulfide minerals compared to OC_{petro} (Bolton et al., 2006; Petsch et al., 2000; Wildman et al., 2004). Indeed, the soil profiles from the East River suggest the OC_{petro} and Re reaction front (Figure 4b) is shallower (~ 60 – 70 cm) than the sulfide reaction front, which is ~ 2 – 4 m depth at a nearby site (Wan et al., 2019, 2021). These observations help to explain the changes in ion ratios with discharge (Figure 3). At high flow, younger surface waters may flow through weathered materials where sulfides have been more depleted, but Re and OC_{petro} have not (Figure 6b), while at mid-to base flow, a higher contribution of ions derived from sulfide-oxidation might be expected. This would act to increase $[Re]/[SO_4^{2-}]$ ratios with runoff (Figure 3).

Another explanation for the patterns in the data would be to invoke secondary processes operating during weathering that alter the dissolved $[Re]$, $[SO_4^{2-}]$, and $[Na^+]$ and their respective ratios. These include the role of cation exchange (Tipper et al., 2021), which for shale bedrocks could influence the measured $[Na^+]$. One might expect that cation exchange could operate when young, Na-depleted surface waters interact with exchange sites on sediments at high flow. However, the C-Q relationship for Na^+ (Figure 2b) shows notable dilution, so it is difficult to invoke this process here. Alternatively, secondary mineral formation could play a role, although Re is not thought to be removed from solution into secondary iron oxy-hydroxide phases during weathering (Horan et al., 2020), both dissolved Re and SO_4 could be prone to reduction (Turchyn et al., 2013) and immobilization of ions in deeper, anoxic flow paths (Calmels et al., 2011). However, it is difficult to invoke these processes to change the $[Re]/[SO_4^{2-}]$ and $[Re]/[Na^+]$ patterns observed here. In the future, additional insight may come from paired analysis of dissolved Re with other redox-sensitive trace metals, or indeed Re isotopes (Dellinger et al., 2021).

In summary, we can explain the higher $[Re]/[SO_4^{2-}]$ and $[Re]/[Na^+]$ ratios at higher water discharge by considering the hydrological pathways operating and the distribution of OC_{petro} , Re, and sulfide minerals in the shallow subsurface (Figures 4 and 6). The data support that Re is derived from reactions happening where gaseous and dissolved O_2 can react with OC_{petro} (Jaffe et al., 2002), which are likely to be closer to the surface in the unsaturated zone, where water resides for shorter periods of time. The conceptual model we put forward builds on those proposed for shale catchments from the perspective of solutes from sulfide oxidation and carbonate and silicate mineral weathering (Winnick et al., 2017; Zhi et al., 2019). Our observations also suggest that Re (and other redox-cycling elements) may provide a useful insight as a tracer of water flow through the vadose zone. When combined with more traditional water source tracers (e.g., Cl^- , stable isotopes of river water), redox-sensitive trace elements could provide improved insight on water pathways in river catchments (Knapp et al., 2020). That said, it is important to note that this behavior may be catchment specific, and depend upon the Re, OC_{petro} , and sulfide content of rocks, while the denudation rate and water table depth will together set the depth of the oxidative weathering fronts (Bolton et al., 2006; Brantley et al., 2013; Gu et al., 2020; Soulet et al., 2021; Wan et al., 2019).

4.3. Dissolved Re Yields and Oxidative Weathering of OC_{petro}

For the Swiss Rivers, the dissolved Re yields (Table S3 in Data Set S1) are 1.6 times higher in the Erlenbach ($1.24^{+0.05}_{-0.04} \times 10^{-2} \text{ mol km}^{-2} \text{ yr}^{-1}$) than the Vogelbach ($0.79^{+0.01}_{-0.01} \times 10^{-2} \text{ mol km}^{-2} \text{ yr}^{-1}$). The suspended sediment yield in the Erlenbach (1986–1989 = $1225 \text{ t km}^{-2} \text{ yr}^{-1}$) is 1.7 times higher than the Vogelbach ($725 \text{ t km}^{-2} \text{ yr}^{-1}$). These new measurements agree with observations from mountain rivers in Taiwan, where dissolved Re yields are correlated with physical erosion rate (Hilton et al., 2014). We note that the instantaneous $[Re]$ values are not linked to suspended sediment concentration at the time of sampling, because $[Re]$ is negatively correlated with runoff (Figure 2c) while suspended sediment concentration increases as

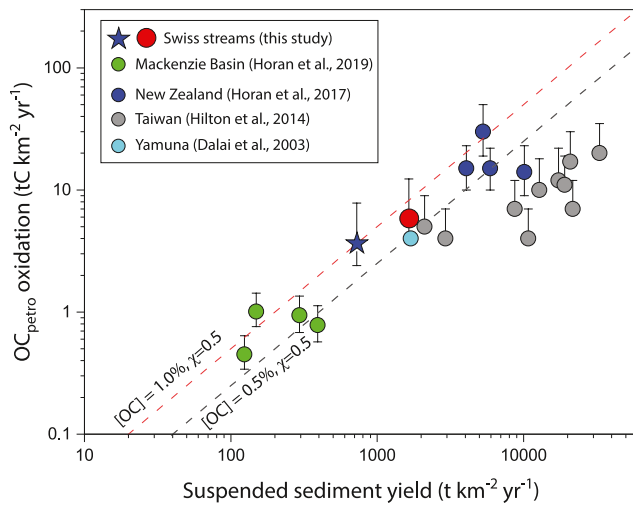


Figure 7. Rock organic carbon (OC_{petro}) oxidation yield ($tC\ km^{-2}\ yr^{-1}$) derived from the rhenium proxy for the Erlenbach (red circle) and Vogelbach (blue star) in the context of published data, versus suspended sediment yield ($t\ km^{-2}\ yr^{-1}$). Dashed lines show the OC_{petro} oxidation rate assuming weathering of only the mass of eroded suspended sediment, for content of 1.0% and 0.5%, assuming a depletion of χ in the OC_{petro} content of eroded sediment of 0.5.

a power law function of runoff (Keller & Weibel, 1991). Therefore, the link to sediment yield operates over longer timescales than single runoff events, associated with those of weathering reactions.

The 2011–2012 calculated dissolved Re yields (J_{Re} , $g\ km^{-2}\ yr^{-1}$) for the Erlenbach and Vogelbach can be used to estimate the corresponding rate of OC_{petro} oxidation ($J_{OC_{\text{petro-ox}}}$, $tC\ km^{-2}\ yr^{-1}$) (Hilton et al., 2014; Horan et al., 2019) using:

$$J_{OC_{\text{petro-ox}}} = J_{\text{Re}} \times \left(\frac{[OC]}{[Re]} \right)_{\text{rock}} \times f_c \times (1 - f_{\text{graphite}}) \quad (3)$$

where $[OC]/[Re]_{\text{rock}}$ is the ratio in sedimentary rocks being weathered ($g\ g^{-1}$), f_c reflects the proportion of the dissolved Re flux derived from OC_{petro} , and f_{graphite} accounts for a fraction of graphitic carbon in the rocks that may be resilient to oxidation (Horan et al., 2019).

For the Erlenbach and Vogelbach we have measurements of $[OC]/[Re]_{\text{rock}}$ (Table S4 in Data Set S1) and a qualitative assessment of f_c from dissolved ion ratios (Figure 5). This suggests that for moderate to high flows, ~ 70 – 90% of the Re is sourced from OC_{petro} (i.e., f_c is 0.7 – 0.9). We have no constraint on f_{graphite} in this setting, so we do not account for this term here. For the Erlenbach and Vogelbach, the OC_{petro} oxidation flux, $J_{OC_{\text{petro-ox}}}$, is calculated via Monte Carlo simulation (10,000 iterations) that accounts for the measured variability in J_{Re} and $[OC]/[Re]_{\text{rock}}$ and f_c values from 0.7 to 0.9 and reported as the median $\pm 1SD$ bounds. For the East River, we use the flux-weighted J_{Re} estimate and a value of 1 for f_c

(Figure 5), but note that the corresponding $J_{OC_{\text{petro-ox}}}$ is more uncertain. This is because the deepest samples from the soil profile ($[Re] = 6.42\ \text{ppb}$) may not represent the unweathered rocks. Recent work in the catchment has shown weathering fronts over several meters in the subsurface (Wan et al., 2019, 2021). This observation, and the inference that rock organic carbon may be contributing to deep soil CO_2 fluxes at the Bradley Meadows site (Winnick et al., 2020), mean that the deepest soil samples (Figure 4) are likely to have undergone some weathering. Therefore, the $[OC]/[Re]_{\text{rock}}$ based on the deepest sample in the weathering profile is not well constrained.

The estimated $J_{OC_{\text{petro-ox}}}$ values based on dissolved Re fluxes for 2011–2012 for the Erlenbach and Vogelbach are $5.7^{+6.6}_{-2.0}\ tC\ km^{-2}\ yr^{-1}$ and $3.6^{+4.2}_{-1.2}\ tC\ km^{-2}\ yr^{-1}$, respectively. For the East River, $J_{OC_{\text{petro-ox}}} \sim 2.5\ tC\ km^{-2}\ yr^{-1}$. These are lower than OC_{petro} oxidation yields estimated for Taiwan and New Zealand using the Re proxy where erosion rates are higher (Hilton et al., 2014; Horan et al., 2017). However, they are higher than those from the Mackenzie River Basin where physical erosion rates are less rapid (Horan et al., 2019), and fit a general, global pattern of increasing OC_{petro} oxidation with erosion rate (Figure 7) (Hilton et al., 2014). The scatter in the global compilation may reflect the OC_{petro} content of bedrocks and/or physical and chemical factors that may protect OC_{petro} from oxidation (Galvez et al., 2020; Hilton & West, 2020). However, recent work has shown that climatic factors (temperature and hydrology) can also control oxidative weathering rates and the resultant CO_2 flux (Soulet et al., 2021; Tune et al., 2020). Unraveling the relative roles of erosion and climate on CO_2 emissions from sedimentary rocks thus remains a research priority.

In terms of the net CO_2 exchange associated with erosion and weathering, the oxidative weathering flux is lower than the export of biospheric organic carbon by the Erlenbach of $14.0 \pm 4.4\ tC\ km^{-2}\ yr^{-1}$ (Smith et al., 2013), which is higher if coarse debris is also considered (Turowski et al., 2016). This potential pathway of CO_2 drawdown (Galy et al., 2015) is greater than the median $+\sigma$ value of $J_{OC_{\text{petro-ox}}}$ for the Erlenbach. The fate of this carbon downstream of this headwater catchment is not known, which makes the overall impact on the carbon cycle difficult to assess (Clark et al., 2017; Hilton & West, 2020). For instance, if the eroded OC_{petro} and biospheric OC escapes degradation during transit (Scheingross et al., 2019) and is delivered to a long-lived sedimentary deposit, the organic carbon cycle would act as a net sink of CO_2 by erosion. However, the median $J_{OC_{\text{petro-ox}}}$ value for the Erlenbach is lower than the corresponding estimates of unweathered OC_{petro} export in the solid load of the river of $10.1 \pm 1.6\ tC\ km^{-2}\ yr^{-1}$ (Smith et al., 2013). Overall,

the analysis here suggests that the weathering intensity of OC_{petro} (i.e., the oxidative weathering flux normalized by the sum of the oxidative weathering flux and OC_{petro} export in river sediments) is $\sim 40\%$ in this catchment, meaning a significant flux of OC_{petro} is still potentially available for weathering downstream. If some of the solid load OC_{petro} exported by these catchments is retained in floodplains (Fox et al., 2020) and oxidized during continental transit (e.g., Bouchez et al., 2010), and the biospheric carbon yield remains similar downstream (e.g., Galy et al., 2007), then erosion could instead act as a source of CO_2 . To assess the global impact of OC_{petro} oxidation on the carbon cycle, we clearly require more catchment-based estimates, with those that examine erosion and weathering fluxes in headwater and mountain catchments, and also as rivers transit large floodplains.

5. Conclusions

We explore the mobility of Re and oxidative weathering in three alpine catchments underlain by sedimentary rocks. Two catchments in Switzerland (Erlenbach and Vogelbach) have similar geology and climate, but contrast in their erosion rates. We find that dissolved Ca^{2+} fluxes are similar between the catchments over the study period 2011–2012, but that the dissolved products of oxidative weathering (e.g., SO_4^{2-} from sulfides and Re from OC_{petro}) have higher fluxes in the more erosive Erlenbach catchment. This is consistent with the inference that oxidation of sulfides and rock organic matter are supply limited in many locations and rates of oxidative weathering can increase with physical erosion rate.

We examine the ratio of dissolved Re to elements derived from silicate mineral weathering (Na^+) and sulfide oxidation (SO_4^{2-}). When compared to other published measurements, the Re in these rivers is dominated by an OC_{petro} source. We find a positive correlation between $[Re]/[Na^+]$ and $[Re]/[SO_4^{2-}]$ ratios and daily runoff in the Erlenbach, Vogelbach, and East River catchments: dissolved Re is relatively enriched at higher river flow. We discuss this common behavior in the context of hydrological pathways and weathering reactions (Figure 6). We suggest that in these catchments, Re is mobilized from a near surface zone where OC_{petro} persists. Overall, the behavior of Re in these shale catchments supports the use of this element as a tracer of OC_{petro} oxidation.

We apply the Re proxy of OC_{petro} oxidation and CO_2 emissions, with the Erlenbach catchment returning an estimate of $5.7^{+6.6}_{-2.0} \text{ tC km}^{-2} \text{ yr}^{-1}$. This is lower than the export of unweathered OC_{petro} ($10.1 \pm 1.6 \text{ tC km}^{-2} \text{ yr}^{-1}$) and biospheric carbon ($14.0 \pm 4.4 \text{ tC km}^{-2} \text{ yr}^{-1}$) in the suspended solid load of this headwater catchment. Our work calls for more catchment-based estimates of OC_{petro} oxidation and an improved understanding of the fate of OC_{petro} as rivers transport sediment downstream.

Conflict of Interest

The authors declare no conflicts of interest relevant to this study.

Data Availability Statement

All data created by this study can be found at the National Geoscience Data Centre (NGDC) at <https://doi.org/10.5285/90c2e879-192e-44d7-ae2b-e9e73de80eae>. Water discharge data for the Erlenbach and Vogelbach Rivers is available at <https://www.envodat.ch/dataset/longterm-hydrological-observatory-alptal-central-switzerland> and for the East River at <https://doi.org/10.21952/WTR/1495380>.

References

- Anderson, S. P., Dietrich, W. E., Torres, R., Montgomery, D. R., & Loague, K. (1997). Concentration–discharge relationships in runoff from a steep, unchanneled catchment. *Water Resources Research*, 33(1), 211–225. <https://doi.org/10.1029/96WR02715>
- Barnes, R. T., Butman, D. E., Wilson, H. F., & Raymond, P. A. (2018). Riverine export of aged carbon driven by flow path depth and residence time. *Environmental Science & Technology*, 52(3), 1028–1035. <https://doi.org/10.1021/acs.est.7b04717>
- Baronas, J. J., Torres, M. A., Clark, K. E., & West, A. J. (2017). Mixing as a driver of temporal variations in river hydrochemistry: 2. Major and trace element concentration dynamics in the Andes–Amazon transition. *Water Resources Research*, 53, 3120–3145. <https://doi.org/10.1002/2016WR019729>
- Berner, R. A., & Canfield, D. E. (1989). A new model for atmospheric oxygen over Phanerozoic time. *American Journal of Science*, 289(4), 333–361. <https://doi.org/10.2475/ajs.289.4.333>

Acknowledgments

This research was funded by a European Research Council Starting Grant (ERC-StG, 678779, ROC- CO_2) to RGH and a Natural Environment Research Council, UK, New Investigator Grant (NERC, NE/I001719/1) to RGH. MW was funded in part through the National Science Foundation (EAR-2103520). MD was in part supported by a COFUND Junior Research Fellowship. This material is partially based upon work supported through the Lawrence Berkeley National Laboratory's Watershed Function Scientific Focus Area. The U.S. Department of Energy (DOE), Office of Science, Office of Biological and Environmental Research funded the work under contract DE-AC02-05CH11231 (Lawrence Berkeley National Laboratory; operated by the University of California) and DE-SC0018155 (to KM and CL). We thank J. Smith for access to samples, C. Ottley and K. Melvin for additional laboratory support, the Science Director and Research Committee of the Rocky Mountain Biological Laboratory, and J. Knapp, X. Gu and two anonymous referees for comments that helped us improve the manuscript.

- Bolton, E. W., Berner, R. A., & Petsch, S. T. (2006). The weathering of sedimentary organic matter as a control on atmospheric O₂: II. Theoretical modeling. *American Journal of Science*, 306, 575–615. <https://doi.org/10.2475/08.2006.01>
- Bouchez, J., Beyssac, O., Galy, V., Gaillardet, J., France-Lanord, C., Maurice, L., & Moreira-Turcq, P. (2010). Oxidation of petrogenic organic carbon in the Amazon floodplain as a source of atmospheric CO₂. *Geology*, 38, 255–258. <https://doi.org/10.1130/G30608.1>
- Brantley, S. L., Holleran, M. E., Jin, L., & Bazilevskaya, E. (2013). Probing deep weathering in the Shale Hills Critical Zone Observatory, Pennsylvania (USA): The hypothesis of nested chemical reaction fronts in the subsurface. *Earth Surface Processes and Landforms*, 38, 1280–1298.
- Brookins, D. G. (1986). Rhenium as analog for fissiogenic technetium: Eh-pH diagram (25°C, 1 bar) constraints. *Applied Geochemistry*, 1, 513–517. [https://doi.org/10.1016/0883-2927\(86\)90056-9](https://doi.org/10.1016/0883-2927(86)90056-9)
- Calmels, D., Gaillardet, J., Brenot, A., & France-Lanord, C. (2007). Sustained sulfide oxidation by physical erosion processes in the Mackenzie River basin: Climatic perspectives. *Geology*, 35, 1003. <https://doi.org/10.1130/G24132A.1>
- Calmels, D., Galy, A., Hovius, N., Bickle, M., West, A. J., Chen, M. C., & Chapman, H. (2011). Contribution of deep groundwater to the weathering budget in a rapidly eroding mountain belt, Taiwan. *Earth and Planetary Science Letters*, 303, 48–58. <https://doi.org/10.1016/j.epsl.2010.12.032>
- Carroll, R. W. H., Bearup, L. A., Brown, W., Dong, W., Bill, M., & Williams, K. H. (2018). Factors controlling seasonal groundwater and solute flux from snow-dominated basins. *Hydrological Processes*, 32, 2187–2202. <https://doi.org/10.1002/hyp.13151>
- Clark, K. E., Hilton, R. G., West, A. J., Robles Caceres, A., Gröcke, D. R., Marthews, T. R., et al. (2017). Erosion of organic carbon from the Andes and its effects on ecosystem carbon dioxide balance. *Journal of Geophysical Research: Biogeosciences*, 122, 449–469. <https://doi.org/10.1002/2016JG003615>
- Cohen, A. S., Coe, A. L., Bartlett, J. M., & Hawkesworth, C. J. (1999). Precise Re-Os ages of organic-rich mudrocks and the Os isotope composition of Jurassic seawater. *Earth and Planetary Science Letters*, 167, 159–173. [https://doi.org/10.1016/S0012-821X\(99\)00026-6](https://doi.org/10.1016/S0012-821X(99)00026-6)
- Colodner, D., Sachs, J., Ravizza, G., Turekian, K., Edmond, J., & Boyle, E. (1993). The geochemical cycle of rhenium: A reconnaissance. *Earth and Planetary Science Letters*, 117, 205–221. [https://doi.org/10.1016/0012-821X\(93\)90127-U](https://doi.org/10.1016/0012-821X(93)90127-U)
- Colodner, D. C., Boyle, E. A., Edmond, J. M., & Thomson, J. (1992). Post-depositional mobility of platinum, iridium and rhenium in marine sediments. *Nature*, 358, 402–404. <https://doi.org/10.1038/358402a0>
- Crusius, J., Calvert, S., Pedersen, T., & Sage, D. (1996). Rhenium and molybdenum enrichments in sediments as indicators of oxic, suboxic and sulfidic conditions of deposition. *Earth and Planetary Science Letters*, 145, 65–78. [https://doi.org/10.1016/S0012-821X\(96\)00204-X](https://doi.org/10.1016/S0012-821X(96)00204-X)
- Crusius, J., & Thomson, J. (2003). Mobility of authigenic rhenium, silver, and selenium during postdepositional oxidation in marine sediments. *Geochimica et Cosmochimica Acta*, 67, 265–273. [https://doi.org/10.1016/S0016-7037\(02\)01075-X](https://doi.org/10.1016/S0016-7037(02)01075-X)
- Dalai, T. K., Singh, S. K., Trivedi, J. R., & Krishnaswami, S. (2002). Dissolved rhenium in the Yamuna River System and the Ganga in the Himalaya: Role of black shale weathering on the budgets of Re, Os, and U in rivers and CO₂ in the atmosphere. *Geochimica et Cosmochimica Acta*, 66, 29–43. [https://doi.org/10.1016/S0016-7037\(01\)00747-5](https://doi.org/10.1016/S0016-7037(01)00747-5)
- Dellinger, M., Hilton, R. G., & Nowell, G. M. (2020). Measurements of rhenium isotopic composition in low-abundance samples. *Journal of Analytical Atomic Spectrometry*, 35, 377–387. <https://doi.org/10.1039/c9ja00288j>
- Dellinger, M., Hilton, R. G., & Nowell, G. M. (2021). Fractionation of rhenium isotopes in the Mackenzie River basin and insights on oxidative weathering. *Earth and Planetary Science Letters*, 573, 117131. <https://doi.org/10.1016/j.epsl.2021.117131>
- Derry, L. A., & France-Lanord, C. (1996). Neogene growth of the sedimentary organic carbon reservoir. *Paleoceanography*, 11(3), 267–275. <https://doi.org/10.1029/95pa03839>
- Dustin, M. K., Bargar, J. R., Jew, A. D., Harrison, A. L., Joe-Wong, C., Thomas, D. L., et al. (2018). Shale Kerogen: Hydraulic Fracturing Fluid Interactions and Contaminant Release. *Energy & Fuels*, 32(9), 8966–8977. <https://doi.org/10.1021/acs.energyfuels.8b01037>
- Fox, P. M., Bill, M., Heckman, K., Conrad, M., Anderson, C., Keilueit, M., & Nico, P. S. (2020). Shale as a source of organic carbon in floodplain sediments of a mountainous watershed. *Journal of Geophysical Research: Biogeosciences*, 125, e2019JG005419. <https://doi.org/10.1029/2019JG005419>
- Gaillardet, J., Dupré, B., Louvat, P., & Allègre, C. J. (1999). Global silicate weathering and CO₂ consumption rates deduced from the chemistry of large rivers. *Chemical Geology*, 159, 3–30. [https://doi.org/10.1016/S0009-2541\(99\)00031-5](https://doi.org/10.1016/S0009-2541(99)00031-5)
- Galvez, M. E., Fischer, W. W., Jaccard, S. L., & Eglinton, T. I. (2020). Materials and pathways of the organic carbon cycle through time. *Nature Geoscience*, 13, 535–546. <https://doi.org/10.1038/s41561-020-0563-8>
- Galy, A., & France-Lanord, C. (1999). Weathering processes in the Ganges-Brahmaputra basin and the riverine alkalinity budget. *Chemical Geology*, 159, 31–60. [https://doi.org/10.1016/S0009-2541\(99\)00033-9](https://doi.org/10.1016/S0009-2541(99)00033-9)
- Galy, V., Beyssac, O., France-Lanord, C., & Eglinton, T. (2008). Recycling of graphite during Himalayan erosion: A geological stabilization of carbon in the crust. *Science*, 322(5903), 943–945. <https://doi.org/10.1126/science.1161408>
- Galy, V., France-Lanord, C., Beyssac, O., Faure, P., Kudrass, H., & Palhol, F. (2007). Efficient organic carbon burial in the Bengal fan sustained by the Himalayan erosional system. *Nature*, 450, 407–410. <https://doi.org/10.1038/nature06273>
- Galy, V., Peucker-Ehrenbrink, B., & Eglinton, T. (2015). Global carbon export from the terrestrial biosphere controlled by erosion. *Nature*, 521, 204–207. <https://doi.org/10.1038/nature14400>
- Gaskill, D. L., Godwin, L. H., & Mutschler, F. E. (1967). *Geologic map of the Oh-Be-Joyful quadrangle, Gunnison County, Colorado, geologic quadrangle map GQ-578*. U.S. Geol. Surv.
- Godsey, S. E., Kirchner, J. W., & Clow, D. W. (2009). Concentration-discharge relationships reflect chemostatic characteristics of US catchments. *Hydrological Processes*, 23(13), 1844–1864. <https://doi.org/10.1002/hyp.7315>
- Gu, X., Rempe, D. M., Dietrich, W. E., West, A. J., Lin, T.-C., Jin, L., & Brantley, S. L. (2020). Chemical reactions, porosity, and microfracturing in shale during weathering: The effect of erosion rate. *Geochimica et Cosmochimica Acta*, 269, 63–100. <https://doi.org/10.1016/j.gca.2019.09.044>
- Hagedorn, F., Schleppi, P., Waldner, P., & Flühler, H. (2000). Export of dissolved organic carbon and nitrogen from Gleysol dominated catchments - The significance of water flow paths. *Biogeochemistry*, 50(2), 137–161. <https://doi.org/10.1023/A:1006398105953>
- Hayes, J. M., Strauss, H., & Kaufman, A. J. (1999). The abundance of ¹³C in marine organic matter and isotopic fractionation in the global biogeochemical cycle of carbon during the past 800 Ma. *Chemical Geology*, 161, 103–125. [https://doi.org/10.1016/S0009-2541\(99\)00083-2](https://doi.org/10.1016/S0009-2541(99)00083-2)
- Hegg, C., McArde, B. W., & Badoux, A. (2006). One hundred years of mountain hydrology in Switzerland by the WSL. *Hydrological Processes*, 20, 371–376. <https://doi.org/10.1002/hyp.6055>
- Hemingway, J. D., Hilton, R. G., Hovius, N., Eglinton, T. I., Haghipour, N., Wacker, L., et al. (2018). Microbial oxidation of lithospheric organic carbon in rapidly eroding tropical mountain soils. *Science*, 360, 209–212. <https://doi.org/10.1126/science.aao6463>
- Hilton, R. G., Gaillardet, J. Ö., Calmels, D., & Birck, J. L. (2014). Geological respiration of a mountain belt revealed by the trace element rhenium. *Earth and Planetary Science Letters*, 403, 27–36. <https://doi.org/10.1016/j.epsl.2014.06.021>

- Hilton, R. G., Galy, A., Hovius, N., Horng, M.-J., & Chen, H. (2011). Efficient transport of fossil organic carbon to the ocean by steep mountain rivers: An orogenic carbon sequestration mechanism. *Geology*, 39(1), 71–74. <https://doi.org/10.1130/G31352.1>
- Hilton, R. G., & West, A. J. (2020). Mountains, erosion and the carbon cycle. *Nature Reviews Earth & Environment*, 1(6), 284–299. <https://doi.org/10.1038/s43017-020-0058-6>
- Horan, K., Hilton, R. G., Dellinger, M., Tipper, E., Galy, V., Calmels, D., et al. (2019). Carbon dioxide emissions by rock organic carbon oxidation and the net geochemical carbon budget of the Mackenzie River Basin. *American Journal of Science*, 319, 473–499. <https://doi.org/10.2475/06.2019.02>
- Horan, K., Hilton, R. G., McCoy-West, A. J., Selby, D., Tipper, E. T., Hawley, S., & Burton, K. W. (2020). Unravelling the controls on the molybdenum isotope ratios of river waters. *Geochemical Perspectives Letters*, 13, 1–6. <https://doi.org/10.7185/geochemlet.2005>
- Horan, K., Hilton, R. G., Selby, D., Ottley, C. J., Gröcke, D. R., Hicks, M., & Burton, K. W. (2017). Mountain glaciation drives rapid oxidation of rock-bound organic carbon. *Science Advances*, 3. <https://doi.org/10.1126/sciadv.1701107>
- Hsu, H. T., Lawrence, C. R., Winnick, M. J., Bargar, J. R., & Maher, K. (2018). A molecular investigation of soil organic carbon composition across a subalpine catchment. *Soil Systems*, 2, 6. <https://doi.org/10.3390/soils2010006>
- Hubbard, S. S., Williams, K. H., Agarwal, D., Banfield, J., Beller, H., Bouskill, N., et al. (2018). The East River, Colorado, Watershed: A mountainous community testbed for improving predictive understanding of multiscale hydrological-biogeochemical dynamics. *Vadose Zone Journal*, 17, 1–25. <https://doi.org/10.2136/vzj2018.03.0061>
- Ibarra, D. E., Moon, S., Caves, J. K., Chamberlain, C. P., & Maher, K. (2017). Concentration–discharge patterns of weathering products from global rivers. *Acta Geochimica*, 36, 405–409. <https://doi.org/10.1007/s11631-017-0177-z>
- Jaffe, L. A., Peucker-Ehrenbrink, B., & Petsch, S. T. (2002). Mobility of rhenium, platinum group elements and organic carbon during black shale weathering. *Earth and Planetary Science Letters*, 198, 339–353. [https://doi.org/10.1016/S0012-821X\(02\)00526-5](https://doi.org/10.1016/S0012-821X(02)00526-5)
- Keller, C. K., & Bacon, D. H. (1998). Soil respiration and georespiration distinguished by transport analyses of vadose CO₂, ¹³CO₂, and ¹⁴CO₂. *Global Biogeochemical Cycles*, 12, 361–372. <https://doi.org/10.1029/98GB00742>
- Keller, H. M., & Weibel, P. (1991). *Suspended sediments in streamwater: Indicators of erosion and bed load transport in mountainous basins*. IAHS Publication (International Association of Hydrological Sciences).
- Kirchner, J. W. (2016). Aggregation in environmental systems—Part 1: Seasonal tracer cycles quantify young water fractions, but not mean transit times, in spatially heterogeneous catchments. *Hydrology and Earth System Sciences*, 20, 279–297. <https://doi.org/10.5194/hess20-279-2016>
- Knapp, J. L. A., von Freyberg, J., Studer, B., Kiewiet, L., & Kirchner, J. W. (2020). Concentration-discharge relationships vary among hydrological events, reflecting differences in event characteristics. *Hydrology and Earth System Sciences*, 24(5), 2561–2576. <https://doi.org/10.5194/hess-20-279-2016>
- Lawrence, C. R., Beem-Miller, J., Hoyt, A. M., Monroe, G., Sierra, C. A., Stoner, S., et al. (2020). An open-source database for the synthesis of soil radiocarbon data: International Soil Radiocarbon Database (ISRad) version 1.0. *Earth System Science Data*, 12, 61–76. <https://doi.org/10.5194/essd-12-61-2020>
- Longbottom, T. L., & Hockaday, W. C. (2019). Molecular and isotopic composition of modern soils derived from kerogen-rich bedrock and implications for the global C cycle. *Biogeochemistry*, 143, 239–255. <https://doi.org/10.1007/s10533-019-00559-4>
- Lupker, M., France-Lanord, C., Lavé, J., Bouchez, J., Galy, V., Métivier, F., et al. (2011). A Rouse-based method to integrate the chemical composition of river sediments: Application to the Ganga basin. *Journal of Geophysical Research*, 116. <https://doi.org/10.1029/2010JF001947>
- Maher, K. (2011). The role of fluid residence time and topographic scales in determining chemical fluxes from landscapes. *Earth and Planetary Science Letters*, 312, 48–58.
- Maher, K., & Druhan, J. (2014). Relationships between the transit time of water and the fluxes of weathered elements through the critical zone. *Procedia Earth and Planetary Science*, 10, 16–22. <https://doi.org/10.1016/j.epsl.2011.09.040>
- Maher, K., Steefel, C. I., DePaolo, D. J., & Viani, B. E. (2006). The mineral dissolution rate conundrum: Insights from reactive transport modelling of U isotopes and pore fluid chemistry in marine sediments. *Geochimica et Cosmochimica Acta*, 70(2), 337–363. <https://doi.org/10.1016/j.gca.2005.09.001>
- McDonnell, J. J., McGuire, K., Aggarwal, P., Beven, K. J., Biondi, D., Destouni, G., et al. (2010). How old is stream water? Open questions in catchment transit time conceptualization, modelling and analysis. *Hydrological Processes*, 24(12), 1745–1754. <https://doi.org/10.1016/j.proeps.2014.08.004>
- Miller, C. A., Peucker-Ehrenbrink, B., Walker, B. D., & Marcantonio, F. (2011). Re-assessing the surface cycling of molybdenum and rhenium. *Geochimica et Cosmochimica Acta*, 75, 7146–7179. <https://doi.org/10.1016/j.gca.2011.09.005>
- Morrison, S. J., Goodknight, C. S., Tigar, A. D., Bush, R. P., & Gil, A. (2012). Naturally occurring contamination in the Mancos Shale. *Environmental Science and Technology*, 46, 1379–1387. <https://doi.org/10.1021/es203211z>
- Parameter-elevation Regressions on Independent Slopes Model (PRISM) Climate Group. (2013). *Average annual precipitation 1981–2010*. Oregon State Univ. Retrieved from <http://www.prism.oregonstate.edu/normals/>
- Petsch, S. T. (2013). Weathering of organic carbon. In *Treatise on geochemistry* (2nd ed.). <https://doi.org/10.1016/B978-0-08-095975-7.01013-5>
- Petsch, S. T., Berner, R. A., & Eglinton, T. I. (2000). A field study of the chemical weathering of ancient sedimentary organic matter. *Organic Geochemistry*, 31, 475–487. [https://doi.org/10.1016/S0146-6380\(00\)00014-0](https://doi.org/10.1016/S0146-6380(00)00014-0)
- Reimer, P. J., Brown, T. A., & Reimer, R. W. (2004). Discussion: Reporting and calibration of post-bomb ¹⁴C data. *Radiocarbon*, 46, 1299–1304. <https://doi.org/10.1017/S0033822200033154>
- Rickenmann, D., & McArdell, B. W. (2007). Continuous measurement of sediment transport in the Erlenbach stream using piezoelectric bedload impact sensors. *Earth Surface Processes and Landforms*, 32, 1362–1378. <https://doi.org/10.1002/esp.1478>
- Rickenmann, D., Turowski, J. M., Fritschi, B., Klaiber, A., & Ludwig, A. (2012). Bedload transport measurements at the Erlenbach stream with geophones and automated basket samplers. *Earth Surface Processes and Landforms*, 37, 1000–1011. <https://doi.org/10.1002/esp.3225>
- Rooney, A. D., Selby, D., Lewan, M. D., Lillis, P. G., & Houzay, J. P. (2012). Evaluating Re-Os systematics in organic-rich sedimentary rocks in response to petroleum generation using hydrous pyrolysis experiments. *Geochimica et Cosmochimica Acta*, 77, 275–291. <https://doi.org/10.1016/j.gca.2011.11.006>
- Ross, D. J. K., & Bustin, R. M. (2009). Investigating the use of sedimentary geochemical proxies for paleoenvironment interpretation of thermally mature organic-rich strata: Examples from the Devonian-Mississippian shales, Western Canadian Sedimentary Basin. *Chemical Geology*, 260, 1–19. <https://doi.org/10.1016/j.chemgeo.2008.10.027>
- Scheingross, J. S., Hovius, N., Dellinger, M., Hilton, R. G., Repasch, M., Sachse, D., et al. (2019). Preservation of organic carbon during active fluvial transport and particle abrasion. *Geology*, 47, 958–962. <https://doi.org/10.1130/G46442.1>

- Schleppi, P., Muller, N., Feyen, H., Papritz, A., Bucher, J. B., & Flühler, H. (1998). Nitrogen budgets of two small experimental forested catchments at Alptal, Switzerland. *Forest Ecology and Management*, 101(1–3), 177–185. [https://doi.org/10.1016/S0378-1127\(97\)00134-5](https://doi.org/10.1016/S0378-1127(97)00134-5)
- Schleppi, P., Waldner, P. A., & Stähli, M. (2006). Errors of flux integration methods for solutes in grab samples of runoff water, as compared to flow-proportional sampling. *Journal of Hydrology*, 319, 266–281. <https://doi.org/10.1016/j.jhydrol.2005.06.034>
- Schuerch, P., Densmore, A. L., McArdell, B. W., & Molnar, P. (2006). The influence of landsliding on sediment supply and channel change in a steep mountain catchment. *Geomorphology*, 78, 222–235. <https://doi.org/10.1016/j.geomorph.2006.01.025>
- Selby, D., & Creaser, R. A. (2003). Re-Os geochronology of organic rich sediments: An evaluation of organic matter analysis methods. *Chemical Geology*, 200, 225–240. [https://doi.org/10.1016/S0009-2541\(03\)00199-2](https://doi.org/10.1016/S0009-2541(03)00199-2)
- Smith, J. C., Galy, A., Hovius, N., Tye, A. M., Turowski, J. M., & Schleppi, P. (2013). Runoff-driven export of particulate organic carbon from soil in temperate forested uplands. *Earth and Planetary Science Letters*, 365, 198–208. <https://doi.org/10.1016/j.epsl.2013.01.027>
- Soulet, G., Hilton, R. G., Garnett, M. H., Dellinger, M., Croissant, T., Ogric, M., & Klotz, S. (2018). Technical note: In situ measurement of flux and isotopic composition of CO₂ released during oxidative weathering of sedimentary rocks. *Biogeosciences*, 15, 4087–4102. <https://doi.org/10.5194/bg-15-4087-2018>
- Soulet, G., Hilton, R. G., Garnett, M. H., Roylands, T., Klotz, S., Croissant, T., et al. (2021). Temperature control on CO₂ emissions from the weathering of sedimentary rocks. *Nature Geoscience*, 14, 665–671. <https://doi.org/10.1038/s41561-021-00805-1>
- Sproson, A. D., Selby, D., Gannoun, A., Burton, K. W., Dellinger, M., & Lloyd, J. M. (2018). Tracing the impact of coastal water geochemistry on the Re-Os systematics of macroalgae: Insights from the basaltic terrain of Iceland. *Journal of Geophysical Research: Biogeosciences*, 123, 2791–2806. <https://doi.org/10.1029/2018JG004492>
- Thimonier, A., Schmitt, M., Waldner, P., & Rihm, B. (2005). Atmospheric deposition on Swiss Long-Term Forest Ecosystem Research (LWF) plots. *Environmental Monitoring and Assessment*, 104, 81–118. <https://doi.org/10.1007/s10661-005-1605-9>
- Tipper, E. T., Bickle, M. J., Galy, A., West, A. J., Pomiès, C., & Chapman, H. J. (2006). The short term climatic sensitivity of carbonate and silicate weathering fluxes: Insight from seasonal variations in river chemistry. *Geochimica et Cosmochimica Acta*, 70, 2737–2754. <https://doi.org/10.1016/j.gca.2006.03.005>
- Tipper, E. T., Stevenson, E. I., Alcock, V., Knight, A. C. G., Baronas, J. J., Hilton, R. G., et al. (2021). Global silicate weathering flux overestimated because of sediment–water cation exchange. *Proceedings of the National Academy of Sciences*, 118(1), e2016430118. <https://doi.org/10.1073/pnas.2016430118>
- Torres, M. A., West, A. J., Clark, K. E., Paris, G., Bouchez, J., Ponton, C., et al. (2016). The acid and alkalinity budgets of weathering in the Andes–Amazon system: Insights into the erosional control of global biogeochemical cycles. *Earth and Planetary Science Letters*, 450, 381–391. <https://doi.org/10.1016/j.epsl.2016.06.012>
- Tune, A. K., Druhan, J. L., Wang, J., Bennett, P. C., & Rempe, D. M. (2020). Carbon dioxide production in bedrock beneath soils substantially contributes to forest carbon cycling. *Journal of Geophysical Research: Biogeosciences*, 125, e2020JG005795. <https://doi.org/10.1029/2020JG005795>
- Turchyn, A. V., Tipper, E. T., Galy, A., Lo, J.-K., & Bickle, M. J. (2013). Isotope evidence for secondary sulfide precipitation along the Marsyandi River, Nepal, Himalayas. *Earth and Planetary Science Letters*, 374, 36–46.
- Turowski, J. M., Badoux, A., & Rickenmann, D. (2011). Start and end of bedload transport in gravel-bed streams. *Geophysical Research Letters*, 38. <https://doi.org/10.1029/2010GL046558>
- Turowski, J. M., Böckli, M., Rickenmann, D., & Beer, A. R. (2013). Field measurements of the energy delivered to the channel bed by moving bed load and links to bedrock erosion. *Journal of Geophysical Research: Earth Surface*, 118, 2438–2450. <https://doi.org/10.1016/j.epsl.2013.04.033>
- Turowski, J. M., Hilton, R. G., & Sparkes, R. (2016). Decadal carbon discharge by a mountain stream is dominated by coarse organic matter. *Geology*. <https://doi.org/10.1130/G37192.1>
- Ugland, R. C., Duncan, A. C., Ebling, J. L., & Kretschman, R. G. (1986). *Water resources data for Colorado, water year 1985—Volume 2. Colorado River basin above Dolores River*.
- Von Freyberg, J., Allen, S. T., Seeger, S., Weiler, M., & Kirchner, J. W. (2018). Sensitivity of young water fractions to hydro-climatic forcing and landscape properties across 22 Swiss catchments. *Hydrology and Earth System Sciences*, 22, 3841–3861. <https://doi.org/10.5194/hess-22-3841-2018>
- Wan, J., Tokunaga, T. K., Brown, W., Newman, A. W., Dong, W., Bill, M., et al. (2021). Bedrock weathering contributes to subsurface reactive nitrogen and nitrous oxide emissions. *Nature Geoscience*, 14, 217–224. <https://doi.org/10.1038/s41561-021-00717-0>
- Wan, J., Tokunaga, T. K., Williams, K. H., Brown, W., Dong, W., & Hubbard, S. S. (2019). Predicting sedimentary bedrock subsurface weathering fronts and weathering rates. *Scientific Reports*, 9. <https://doi.org/10.1038/s41598-019-53205-2>
- Wildman, R. A., Berner, R. A., Petsch, S. T., Bolton, E. W., Eckert, J. O., Mok, U., & Evans, J. B. (2004). The weathering of sedimentary organic matter as a control on atmospheric O₂: I. Analysis of a black shale. *American Journal of Science*, 304, 234–249. <https://doi.org/10.2475/ajs.304.3.234>
- Winkler, W., Wildi, W., Van Stuijvenberg, J., & Caron, C. (1985). *Wägital-Flysch et autres flyschs jenniques en Suisse Centrale. Stratigraphie, sédimentologie et comparaisons*. Eclogae Geologicae Helvetiae.
- Winnick, M. J., Carroll, R. W. H., Williams, K. H., Maxwell, R. M., Dong, W., & Maher, K. (2017). Snowmelt controls on concentration-discharge relationships and the balance of oxidative and acid-base weathering fluxes in an Alpine catchment, East River, Colorado. *Water Resources Research*, 53, 2507–2523. <https://doi.org/10.1002/2016WR019724>
- Winnick, M. J., Lawrence, C. R., McCormick, M., Druhan, J. L., & Maher, K. (2020). Soil respiration response to rainfall modulated by plant phenology in a montane meadow, East River, Colorado, USA. *Journal of Geophysical Research: Biogeosciences*, 125, e2020JG005924. <https://doi.org/10.1029/2020JG005924>
- WSL. (2019). Retrieved from <https://www.wsl.ch/en/about-wsl/instrumented-field-sites-and-laboratories/experimented-field-sites-for-natural-hazards/torrent-investigation-in-the-alptal/site-description.html>
- Yeghicheyan, D., Bossy, C., Bouhnik Le Coz, M., Douchet, C., Granier, G., Heimburger, A., et al. (2013). A compilation of silicon, rare earth element and twenty-one other trace element concentrations in the natural river water reference material SLRS-5 (NRC-CNRC). *Geostandards and Geoanalytical Research*, 37, 449–467. <https://doi.org/10.1111/j.1751-908X.2013.00232.x>
- Zhi, W., Li, L., Dong, W., Brown, W., Kaye, J., Steefel, C., & Williams, K. H. (2019). Distinct source water chemistry shapes contrasting concentration-discharge patterns. *Water Resources Research*, 55, 4233–4251. <https://doi.org/10.1029/2018WR024257>